Loss of Lamin A leads to the nuclear translocation of AGO2 and compromised RNA interference

Vivian Lobo[1,2†], Iwona Nowak[1,2†], Carola Fernandez[1,2†], Ana Iris Correa Muler[1,2#], Jakub O. Westholm[3#], Hsiang-Chi Huang[1,2,4], Ivo Fabrik[5], Hang Thuy Huynh[1,2], Melis Kanik[1,2], Anetta Härtlova[2,4], Daniel Benhalevy[6], Davide Angeletti[4,7] and Aishe A. Sarshad[1,2*]

1. Department of Medical Biochemistry and Cell biology, Institute of Biomedicine, University of Gothenburg, SE-40530 Gothenburg, Sweden
2. Wallenberg Centre for Molecular and Translational Medicine, University of Gothenburg, SE-40530 Gothenburg, Sweden
3. Department of Biochemistry and Biophysics, National Bioinformatics Infrastructure Sweden, Science for Life Laboratory, Stockholm University, Box 1031, SE-17121 Solna, Sweden
4. Department of Microbiology and Immunology, Institute of Biomedicine, University of Gothenburg, SE-40530 Gothenburg, Sweden
5. Biomedical Research Centre, University Hospital Hradec Kralove, Sokolska 581, 500 05 Hradec Kralove, Czech Republic
6. Lab of Cellular RNA Biology, The Shmunis School of Biomedicine and Cancer Research, The George S. Wise Faculty of Life Sciences, Tel Aviv University, Tel Aviv, 69978, Israel
7. SciLifeLab, University of Gothenburg, SE-40530 Gothenburg, Sweden

* Corresponding author: Aishe A. Sarshad (aishe.sarshad@gu.se)

† # These authors contributed equally

Keywords: Argonaute 2, Lamin A, EGFR, FAM120A, Src, Y393-AGO2, RNA interference, gene regulation

ABSTRACT

In mammals, RNA interference (RNAi) is mostly studied as a cytoplasmic event, however, numerous reports convincingly show nuclear localization of the AGO proteins. Nevertheless, the mechanism of nuclear entry remains to be fully elucidated, and the extent of nuclear RNAi further explored. We found that reduced Lamin A levels significantly induced nuclear influx of AGO2 in SHSY5Y neuroblastoma and A375 melanoma cancer cell lines, which normally have no nuclear AGO2. The translocation of AGO2 was accompanied by aggravated cell proliferation and we further found that the loss of Lamin A leads to EGFR and Src kinase activation, which regulates the turnover and stability of cytoplasmic AGO2. Furthermore, Lamin A KO significantly reduced the activity of nuclear RNAi. This was evident by AGO fPAR-CLIP in WT and Lamin A KO cells, where we observed ca 60% less efficiency of RNAi. Mass spectrometry of AGO interactome, from the nuclear fraction, indicated that AGO2 is in complex with FAM120A, a known interactor of AGO2 that reduces the activity of RNAi by competing with AGO2 transcript binding. Therefore, loss of Lamin A starts a signaling cascade that mediates nuclear AGO2 translocation to rapidly inhibit RNAi in order to facilitate cancer proliferation.

INTRODUCTION

The eukaryotic genome is enclosed by the nuclear envelope (NE), which is a highly regulated barrier that separates the nucleus from the cytoplasm [1]. One of the major components of the NE are the nuclear Lamins [2], encoded by three highly conserved Lamin genes – *LMNA*, *LMNB1* and *LMNB2* [3]. Alternative splicing of *LMNA* gene results in the production of four different A-type Lamin proteins, where Lamin A and Lamin C are the predominant isoforms [4]. While *LMNB1* and *LMNB2* encoded proteins (B-type Lamins) are ubiquitously expressed, A-type Lamin expression is limited to differentiated cells [3].

A and B type Lamins belong to the type V intermediate protein family and assemble into higher order structures forming the nuclear lamina – a main component of the NE and an important platform for information exchange between the nucleus and cytoplasm [5]. Accordingly, Lamin proteins are highly involved in regulation of gene expression. The Lamins are closely associated with Lamin-associated domains (LADs), genomic regions characterized by densly packed chromatin and transcriptional inactivation [6-7]. Therefore, precise control of the nuclear lamina composition is crucial for safeguarding cellular identity by keeping proper chromatin organization and cellular morphology [8-9].

Gene expression is also regulated post-transcriptionally, among others by RNA interference (RNAi), executed by miRNA-loaded AGO proteins [10-11]. In mammals, miRNA duplexes, matured by DROSHA and DICER enzymatic processing, are loaded in to one of four AGO proteins, comprising the core RNA induced silencing complex (RISC). Based on nucleotide base hybridization, AGO:miRNA RISC target mRNAs, canonically in the cytoplasm [12]. RISC induces RNAi by recruiting key mediating factors, such as TNRC6A-C scaffolding proteins, which bridge the RISC complex with CCR4-NOT deadenylation complex. Additionally, AGO proteins can interact with various proteins that either facilitate gene silencing, e.g., PABPC, DDX6, XRN1, or inhibit the process, such as FAM120A or HuR [13-14].

In mammals, the process of RNAi is generally accepted as a cytoplasmic event [15-16], but numerous reports documented the nuclear localization of the AGO proteins [17-21]. In the nucleus, AGO proteins were suggested to regulate several functions aside from RNAi, including chromatin remodeling, transcriptional regulation, alternative splicing, genome integrity, and DNA repair in cancer cells [18-19; 21-22]. Therefore, AGO molecular function of loading miRNAs and targeting specific RNAs by sequence complementarity, may promote regulation

of several biological processes in a context-dependent manner, based on the cellular environment and RNA and protein interactors.

Another cellular variability in AGO proteins are their post-translational modifications that affect their function. Specifically, AGO2 activity was found to be regulated by the oncogenic kinases EGFR, Src and Akt [23-25]: EGFR and Src kinases inhibit miRNA-directed gene silencing [23-24], while Akt kinase was shown to shift AGO2 activity from transcript degradation to translational repression [25]. Moreover, Akt kinase was suggested to promote cytoplasmic localization of AGO2 in mouse splenocytes [26]. AGO2 activity and localization is also regulated by other RNA binding proteins. Recent studies revealed competitive binding of TNRC6 to various proteins involved in RNA destabilization, such as TRIM71 and UPF1 [27], therefore, RNAi efficiency also depends on the TNRC6 pool available for AGO binding. Nuclear import of AGO:miRNA complexes was linked with Importin 8 in HeLa cells and more recently to FAM172A in mouse embryonic fibroblasts [17, 28-29]. Nevertheless, the underlying molecular mechanisms of AGOs activity, translocation and subsequent RNAi-mediated gene regulation in the nucleus of cancer cells remains to be fully explored. Several groups have explored nuclear AGO2 transcript occupancy distribution and reported substantial occupancy of AGO2 at intronic sites within pre-mRNAs [20, 22, 30]. In stem cells, nuclear RNAi reflected cytoplasmic RNAi, but was significantly more potent [20]. However, most of the literature does not address the level of nuclear AGO-mediated gene silencing.

Herein, we aimed to investigate the crosstalk between the nuclear lamina and its potential to mediate AGO2 nuclear translocation. Since the nuclear envelope is a crucial link in a chain of dialogue between the cytoplasm and the nucleus, its composition is bound to influence nuclear import. However, this is not extensively characterized. Further, the cellular state and factors leading to increased nuclear AGO2 accumulation and regulation are not yet fully elucidated. Despite that the first observation of nuclear AGO2 dates back to 2008 [31], the extent of nuclear AGO2 presence, activity and function remains to be fully explored.

In this study, we identified that loss of Lamin A expression triggers AGO2 nuclear translocation in cancer cells. Moreover, we found that upon the loss of Lamin A, EGFR and Src kinases are enzymatically active, regulating the turnover and stability of cytoplasmic AGO2 and the activity of RNAi.

MATERIAL AND METHODS

Cell culture

HeLa ovarian adenocarcinoma cells (ATCC, CCL-2), MCF7 breast cancer cells (ATCC, HTB-22), CUT09 and STE01 lung cancer cells (kind gift from Ruth Palmer and Bengt Hallberg), Molm13 acute myeloid leukemia cells (DMSZ, ACC 554), Granta-519 B cell lymphoma cells (DMSZ, ACC 342), HEK293 (ATCC, CRL-1573) and HEK293T (ATCC, ACS-4500) embryonic kidney cells, SHSY5Y neuroblastoma cells (ATCC, CRL-2266), HAP1 chronic myeloid leukemia cells (kind gift from Maria Falkenberg), U2OS osteosarcoma cells (ATCC, HTB-96) and A375 melanoma cells (ATCC, CRL-1619) were cultured at 37°C, with 5% CO_2. HeLa, MCF7, HEK293, HEK293T, U2OS and A375 cells were cultured in DMEM media (11995065, Gibco) supplemented with 10% Fetal Bovine Serum (FBS) (10270106, Gibco) and 1% Penicillin-Streptomycin (P/S) solution (15140122, Gibco). CUT09, STE01, Molm13, Granta-519 and SHSY5Y cells were cultured in RPMI media (61870010, Gibco) complemented with 10% FBS and 1% P/S solution. HAP1 cells were cultured in IMDM media (12440053, Gibco) supplemented with 10% FBS and 1% P/S solution. A375 and SHSY5Y Lamin A knock out cells were cultured with respective complete media complemented with 2 µg/ml puromycin (P9620, Sigma Aldrich) and 350 µg/ml G418 (G8168, Sigma Aldrich).

Biochemical fractionation

Cells were fractionated as described in [32] with minor modifications. Briefly, cells were resuspended in Hypotonic Lysis Buffer (HLB) buffer [10 mM Tris, pH 7.5; 10 mM NaCl; 3 mM MgCl2; 0.3% NP-40 (vol/vol); and 10% glycerol (vol/vol)], supplemented with protease and phosphatase inhibitor cocktail (78445, ThermoFisher) by gentle pipetting and left on ice for 5 min. The nuclei were separated by centrifugation at 200 *g* for 2 min and the supernatant was collected as the cytoplasmic lysate. The pellet, containing the nuclear fraction, was further washed three times in HLB buffer and each time collected by centrifugation at 200 *g* for 2 min. The washed nuclear pellet was resuspended with equal volumes of Nuclear Lysis Buffer (NLB) buffer [20 mM Tris, pH 7.5; 150 mM KCl; 3 mM MgCl2; 0.3% NP-40 (vol/ vol), and 10% glycerol (vol/vol)], supplemented with protease and phosphatase inhibitor cocktail. The nuclear lysate was sonicated twice, 10 s on and 30 s off, at 60% amplitude (Sonics, VCX130). Both cytoplasmic and nuclear lysates were further cleared by centrifugation at 21,000 *g* for 15 min.

Western blot analysis

Total protein lysates were prepared by suspending the cell pellets in NP-40 lysis buffer [20 mM Tris, pH 7.5; 150 mM NaCl; 2 mM EDTA; 1% (v/v) NP-40] and incubating on ice for 20 min. Following, the samples were centrifuged at 21,000 *g* for 20 min and the supernatant collected as the total protein lysate. Cytoplasmic and nuclear lysates were prepared as described above. Protein concentration for the total and cytoplasmic lysates were quantified by Bradford Reagent (B6916, Sigma Aldrich) and 10-20 µg of protein was used for western blot experiments. The nuclear lysates were loaded at 1:1 volume ratio with the cytoplasmic fraction, on to 8%-12% Bis-Tris PAGE gels. Following electrophoresis, the proteins were transferred onto Nitrocellulose membrane (1060000, Cytiva) and the blots stained with Ponceau S, washed, and blocked with skimmed milk (70166, Sigma). Membranes were incubated overnight with either of the following antibodies indicated in table below. Following, blots were washed and incubated with HRP conjugated anti-rabbit IgG (NA934, Cytiva) or anti-mouse IgG (NA931, Cytiva). The signal was detected by chemiluminescence using Thermo Scientific SuperSignal™ West Dura Extended Duration Substrate (34076, ThermoFisher).

Antibody	Company	Dilution
anti-AGO2	ab32381 or ab186733, Abcam	1:5000
anti-Lamin B1	ab16048, Abcam	1:10,000
anti-Histone H3	4499, CST	1:10 000
anti-Lamin A	sc-518013, Santacruz	1:1000
anti-Lamin A/C	sc-376248HRP, Santacruz	1:1000
Streptavidin-HRP	S911, Molecular Probes	1:4000
anti-V5	R960-25, Invitrogen	1:4000
anti-FAM120A	ab156695, Abcam	1:2000
anti Src (419)	sc-81521, Santacruz or 6943T, CST	1:1000
anti-Src (530)	sc-166860, Santacruz	1:500
anti-Src	sc-8056, Santacruz	1:1000
anti-EGRF	4267S, CST	1:1000
anti-pY1068 EGFR	2234S, CST	1:1000
anti-PABPC	sc-32318, Santacruz	1:1000
anti-Calreticulin	sc-373863HRP, Santacruz	1:1000
anti-TNRC6	A302-329A, Fortis Life Sciences	1:500
anti-NUP85	sc-376111, Santacruz	1:500

anti-Ubiquitin	sc-8017, Santacruz	1:2000

siRNAs transfection

siRNAs targeting *LMNA* (4392420 and 4390824, assay IDs: s530951 and s8221) and *LMNB1* (4392420, assay IDs: s8224 and s8225), and *NUP85* (4427037, assay IDs: s36611 and s36612) as well as negative control scramble oligonucleotide (4390843), without complementarity to sequences in the human transcriptome, were purchased from ThermoFisher. Cells were seeded one day prior to the siRNA transfections. siRNAs, scramble oligonucleotide and Lipofectamine RNAiMax (13778150, ThermoFisher) were diluted in Opti-MEM reduced media (31985047, Gibco) and added to the cell culture at a final concentration of 7.5 nM. 24 h following the transfection, the media was changed to fresh complete media. After another 24 h of culture, cells were harvested for downstream analysis. Silencing efficiency was assessed by western blot.

CRISPR-Cas9 gene editing

Lamin A knockout cells were generated in A375, SHSY5Y and HeLa cells using PITCH-CRISPR-Cas9-microhomology-mediated end-joining [33]. Briefly, two all-in-one CRISPR-Cas9 vectors were generated from pX330A-1x2 (58766, Addgene) and pX330S-2-PITCh (63670, Addgene), expressing Cas9 nuclease and two gRNAs (see below for sequences) together with the CRIS-PITCh vector pX330S-2-PITCh (63670, Addgene), harboring the Lamin A microhomologies and GFP-Puro or GFP-Neo/Kan insertions, were transiently transfected into A375 and SHSY5Y using JetOptimus transfection reagent (117-01, Polyplus) according to the manufacturer's instructions. Single clones undergoing recombination were selected by complementing culture media with Puromycin at a concentration of 2 µg/ml and G418 at a concentration of 350 µg/ml for 10 days. Homozygous Lamin A knockout were identified by PCR and western blot screening. Genomic DNA was extracted using PureLink™ Genomic DNA (K182002, ThermoFisher) following the manufacture's protocol. PCR was performed using OneTaq polymerase (M0480S, New England Biolabs) following the manufacture's protocol. The primer sequences were as follows: primer 232: GCAGATCAAGCGCCAGAATG; primer 233: GCTTCATGTGGTCGGGGTAA; primer 235: GGGACACTGTCAAGCTCTCC;; primer 281: TTACCCCGACCACATGAAGC; β-Actin Fw: GTCGTCGACAACGGCTCCGGCATGTG, Rv: CATTGTAGAAGGTGTGGTGCCAGAT.

The gRNA sequences targeting *LMNA* Exon 9 locus and a generic PITCh-gRNA were as follows: *LMNA* sgRNA-Ex 9 Fw1: aaacCTACCGACCTGGTGTGGAAGC; *LMNA* sgRNA-Ex 9 Rv1: CACCGCTTCCACACCAGGTCGGTAG; *LMNA* sgRNA-Ex 9 Fw2: CACCGAGTTGATGAGAGCCGTACGC; *LMNA* sgRNA-Ex 9 Rv 2: aaacGCGTACGGCTCTCATCAACTC)

Immunofluorescence staining

Cells were plated at a density of 60,000 cells/cm^2 on glass coverslips inside 12-well dishes. Next day, cells were washed once in 1x PBS and fixed with 4% paraformaldehyde (1267, Solveco) for 15 min at RT. Following, cells were washed with 1x PBS and permeabilized in 0.5% Triton X-100 for 10 min at RT. Subsequently, cells were blocked with 5% BSA (BP9703-100, Fisher Bioreagents) in 1x PBS for 1 h and stained with primary antibodies indicated in the table below. The cells were washed three times in 1x PBS and stained with 1:400 Phalloidin (B3475, Invitrogen), to visualize F-actin, or secondary antibodies indicated in the table below for 1 h at RT. To visualize the DNA within the nucleus, cells were stained with 300 nM 4',6-diamidino-2-phenylindole (DAPI; D1306, Invitrogen) for 5 min at RT. Slides were mounted using ProLong Diamond Antifade Mountant (P36961, Invitrogen). Confocal images were taken on a Zeiss LSM780 and the images analyzed using ImageJ software.

Antibody	Company	Dilution
anti-Lamin B1	ab16048, Abcam	1:500
anti-Pol II	sc-56767 Santa Cruz	1:200
anti-Lamin A	sc-518013, Santacruz	1:400
anti-Histone H3	4499, CST	1:400
anti-V5	R960-25, Invitrogen	1:400
anti-EGFR	4267S, CST	1:400
anti-Src	sc-8056, Santacruz	1:400
anti-Src (419)	sc-81521, Santacruz	1:400
anti-Scr (530)	sc-166860, Santacruz	1:200
anti-FAM120A	ab156695, Abcam	1:400
anti-rabbit Alexa 488	A11008, Invitrogen	1:2000
anti-mouse Alexa 594	A11005, Invitrogen	1:2000

Cell proliferation assay

For cell proliferation assays, A375 and SHSY5Y (WT and Lamin A KO) cells were seeded in 6-well plates at density of 3,125 cells/cm^2 and counted with LUNA-II™ Automated Cell Counter (Logos Biosystems) every 24 h for 6 days. The cells were grown in their respective complete media, which was changed every two days. The experiment was performed in four biological replicates and, additionally, each included two technical replicates. Exponential (Malthusian) growth proliferation assay line was fitted, and doubling time calculated using GraphPad Prism (Version 9.5.1).

Flow cytometry for cell cycle analysis

A375 and SHSY5Y (WT and Lamin A KO) cells were seeded in 6-well plates at a density of 100,000 cells/well and incubated at 37°C overnight. For cell cycle analysis, 50,000 cells were collected and fixed with ice-cold 70% (v/v) ethanol at -20°C overnight. The cells were pelleted at 300 *g* for 5 min and the pellet suspended in PI solution (50 µg/ml Propidium iodide (81845, Sigma Aldrich), 0.1 mg/ml RNase A (EN0531, ThermoFisher), 0.05% Triton X-100 in 1x PBS) for 40 min at 37°C. Cells were then washed with 1x PBS and processed for cell cycle analysis on BD-LSRII LSRII (BD Bioscience). Data was analyzed using FlowJo (Treestar Inc.).

Generation of Y393A-AGO2 plasmid

Point mutation in LJM1-FH-AGO2-WT plasmid (91978, Addgene) in the open reading frame of AGO2 coding sequence, resulting in Y393A mutation, was introduced with Q5® Site-Directed Mutagenesis Kit (E0554S, New England Biolabs) according to manufacturer's instructions. For introducing the mutation the following primers were used: Fw: CCTTCGCACTATCACGTCCTCT; Rv: GCCCGCATACGTGTTCTTCAG. The generated plasmid was verified by sequencing.

Plasmid transfection

Cells were transfected with the following expression plasmids: eGFP-NLS (67652, Addgene), pCDH-CMV-hLamin_A-IRES-copGFP-EF1-puro (132773, Addgene), LJM1-FH-AGO2-WT (91978, Addgene), LJM1-FH-AGO2-Y393A; pDEST40-2XFL-wtSrc (140295, Addgene); pDEST40-2XFL-Src-Y530F (140319, Addgene); pDEST40-2XFL-Src-Y419F (140317, Addgene) or pDEST40-2XFL-Src-K298M (140315; Addgene) using JetOptimus transfection reagent (117-01,

Polyplus) or Lipofectamine 2000 (11668027, Invitrogen) according to manufacturers' instructions. In the case of eGFP-NLS, pDEST40-2XFL-wtSrc, pDEST40-2XFL-Src-Y530F, pDEST40-2XFL-Src-Y419F and pDEST40-2XFL-Src-K298M plasmids the cells were harvested for 24 h post transfection, while for pCDH-CMV-hLamin_A-IRES-copGFP-EF1-puro, LJM1-FH-AGO2-WT and LJM1-FH-AGO2-Y393A plasmids the transfection was prolonged to 48 h. Transfection efficiency was assessed by immunofluorescence staining and/or western blot.

RNA isolation, reverse transcription, and qPCR

Total RNA was extracted using Quick-RNA Miniprep Kit (BioSite-R1055, Zymo Research). RNA concentration was assessed with Implen N60 nanophotometer. Following, 500 ng of RNA was reverse transcribed using iScript™ cDNA Synthesis Kit (1708891, Biorad). For qPCR reactions, cDNA was diluted 50 times. qPCR was performed in XT96 thermocycler with iTaq™ Universal SYBR® Green Supermix (1725124, Biorad) using thermocycling conditions recommended by the manufacturer. The sequences of the primers were as follows: 18S rRNA: Fw: CCCTCCAATGGATCCTCGTT, Rv: AGAAACGGCTACCACATCCA, *AGO2:* Fw: TGAGCTTGCAGGCGTTACAC, Rv: CAAGAGGGTTAGAGCAGCCTT; *LMNA*: Fw: AGACCCTTGACTCAGTAGCC, Rv: AGCCTCCAGGTCCTTCA.

Generation of V5-APEX2-SENP2 expressing cells

V5-APEX2-SENP2 expression was introduced into A375 Lamin A KO and WT cells by lentiviral transduction according to the protocol described by Tandon and colleagues [34]. Cells were transfected with a mixture of viral packaging proteins VSV-G (12259, Addgene), viral backbone psPAX2 plasimd (12260, Addgene) and for the introduction of V5-APEX2-SENP2 (129276, Addgene) were co-transfected at ratio 3:2:4 where the final plasmid concentration in the media is 2,25 µl/ml. Cells were kept in selection media [complete media supplemented with 10 µg/ml Blasticidin (A1113903, Gibco)] for 10 days, when control, none transduced, cells died. Following, cells were cultured in complete media for respective parental cell lines.

Proximity-dependent biotinylation

Cells were grown in 15 cm cell culture dishes until they reached approximately 50% confluency. Following, biotinylation of proteins proximal to V5-APEX2-SENP2 was performed according to previously published protocol [35] with a minor modification where Biotin-Phenol (SML2135,

Sigma-Aldrich) was added to the media at a final concentration of 1 mM and the incubation with Biotin-Phenol was extended to 40 mins.

Streptavidin affinity pull down assay

Following the proximity-dependent biotinylation procedure, cells were lysed in RIPA buffer [50 mM Tris, 150 mM NaCl, 0.1% (w/v) SDS, 0.5% (w/v) sodium deoxycholate and 1% (v/v) Triton X-100] complemented with 10 nM sodium azide (S2002, Sigma-Aldrich), 10 mM sodium ascorbate (A4034, Sigma-Aldrich) and 5 nM of Trolox (238813, Sigma-Aldrich) and protease inhibitor (78439, ThermoFisher). Subsequently, the protein concentration was estimated using Pierce reagent (22660, ThermoFisher), and 250 µg of protein were subjected to streptavidin affinity precipitation using 20 µl streptavidin-coupled magnetic beads (88817, ThermoFisher) at 4°C overnight, under constant rotation, for enrichment of biotinylated proteins. After the incubation, beads were washed with a series of buffers: 2 times with RIPA buffer, once with 1 M KCl (10735874, ThermoFisher), once with 0.1 M Na_2CO_3 (230952, Sigma-Aldrich), once with 2 M Urea (U6504, Sigma-Aldrich) in 10 mM Tris-HCl (15567027, Invitrogen™), freshly prepared, and twice with RIPA buffer. Following the washes, beads were incubated for 10 min at 95°C in 60 µl of 3x Laemmli SDS Sample Buffer (J61337.AC, ThermoFisher) supplemented with 2 nM biotin (B4501, Sigma-Aldrich), to elute bound proteins for subsequent western blot analysis.

Immunoprecipitation assays and AGO protein affinity purification with T6B peptide

For identification of Lamin A and AGO-interacting protein partners, respective proteins were pulled down using either anti-Lamin A antibody, Flag-tagged T6B peptide for AGO1-4 isolation [36], or pAGO2 antibody. Lamin A was immunoprecipitated from 2 mg of total protein lysate in A375 WT and Lamin A KO cells with 3 µg of antibody. AGO1-4 or pAGO2 proteins were pulled down from nuclear or cytoplasmic lysates. Volumes corresponding to 3 mg of cytoplasmic fraction was used together with 400 µg of T6B peptide or 2 µg of pAGO2 antibody. Dynabead Protein G beads (10004D, ThermoFisher) and anti-Flag M2 beads (M8823, Millipore) were conjugated with either anti-Lamin A antibody, pAGO2 antibody or T6B peptide for 4 h, washed and incubated with protein lysates. Next, beads were washed with NP-40 buffer. pAGO2 bound proteins were eluted at 95°C for 5 min in 2× SDS Laemmli buffer and assessed by western blot. Lamin A and T6B bound proteins were eluted by incubation with 0.2 M Glycine, pH 2.5 by gentle shaking for 15 min followed by neutralization of the eluate using 1 M Tris,

pH 8. The pull-down efficiency was confirmed by western blot and the eluate submitted for mass spectrometry analysis at Proteomics Core Facility (University of Gothenburg, Sweden).

Mass spectrometry

Samples eluted after AGO protein and Lamin A affinity purification were processed using modified filter-aided sample preparation (FASP) method [37]. Briefly, samples were reduced in 100 mM dithiothreitol (DTT) at 60°C for 30 min, transferred to Microcon-30kDa Centrifugal Filter Units (MRCF0R030, Merck) and washed several times with 8 M urea and once with digestion buffer (DB; 50 mM TEAB, 0.5% sodium deoxycholate (SDC)) prior to alkylation (10 mM methyl methanethiosulfonate (MMTS) in DB for 30 min at RT. Samples were digested with 0,3 µg Pierce MS grade Trypsin (90057, ThermoFisher) at 37°C overnight and an additional portion of trypsin was added and incubated for another two h. Peptides were collected by centrifugation.

Following, digested peptide samples were labelled using TMT 16-plex isobaric mass tagging reagents (90063, ThermoFisher) for relative quantification. The samples were combined into one TMT-set and SDC was removed by acidification with 10% TFA. The TMT-set was further purified using High Protein and Peptide Recovery Detergent Removal Spin Column (88305, ThermoFisher) and Pierce peptide desalting spin columns (89852, ThermoFisher) according to the manufacturer's instructions, prior to basic reversed-phase chromatography (bRP-LC) fractionation. Peptide separation was performed using a Dionex Ultimate 3000 UPLC system (ThermoFisher) and a reversed-phase XBridge BEH C18 column (3,5 µm, 3.0x150 mm, 186008164, Waters Corporation) with a gradient from 3% to 100% acetonitrile in 10 mM ammonium formate at pH 10.00 over 23 min at a flow of 400 µL/min. The 40 fractions were concatenated into 20 fractions.

The dried samples were reconstituted in 3% acetonitrile and 0,2% formic acid. The TMT fractions in were analyzed on an Orbitrap Lumos Tribrid mass spectrometer interfaced and an Easy-nLC1200 liquid chromatography system (ThermoFisher). Peptides were trapped on an Acclaim Pepmap 100 C18 trap column (100 µm x 2 cm, particle size 5 µm, 164199, ThermoFisher) and separated on an in-house packed analytical column i.d. 75 µm, particle size 3 µm, Reprosil-Pur C18, Dr. Maisch, length 35 cm using a gradient from 3% to 80% acetonitrile in 0.2% formic acid over 85 min at a flow of 300 nL/min. Precursor ion mass spectra were acquired at 120,000 resolution and MS/MS analysis was performed in data-dependent mode

where CID spectra of the most intense precursor ions were recorded in the ion trap at collision energy setting of 35. Precursors were isolated in the quadrupole with a 0,7 m/z isolation window, charge states 2 to 7 were selected for fragmentation, dynamic exclusion was set to 45 s and 10 ppm. MS3 spectra for reporter ion quantitation were recorded at 50,000 resolution, multi-notch isolation with 10 notches and HCD fragmentation collision energy of 55.

Lamin A affinity purification samples were analysed by label free approach on an Orbitrap Exploris 480 mass spectrometer interfaced with an Easy-nLC1200 liquid chromatography system (ThermoFisher) in trap column configuration (see above). Peptides were separated using a gradient from 5% to 45% acetonitrile in 0.2% formic acid over 48 min at a flow of 300 nL/min. Precursor ion mass spectra were acquired at 120,000 resolution and MS/MS analysis was performed in data-dependent mode with HCD collision energy setting of 30. Precursors were isolated in the quadrupole with a 0.7 m/z isolation window, charge states 2 to 6 were selected for fragmentation, dynamic exclusion was set to 30 s and 10 ppm.

Following, the data files were merged for identification and relative quantification using Proteome Discoverer version 2.4 (ThermoFisher). The data matching was against Homo Sapiens (Swissprot) using Mascot version 2.5.1 (Matrix Science) as a search engine. The precursor mass tolerance was set to 5 ppm and fragment mass tolerance to 0,6 Da. Tryptic peptides were accepted with one missed cleavage, variable modifications of methionine oxidation and fixed cysteine alkylation, TMT pro modifications of N-terminal and lysine were selected. Percolator was used for PSM validation with the strict FDR threshold of 1%. Identified proteins were filtered at 1% FDR at protein level. For relative quantification reporter ions were identified in the MS3 HCD spectra with 3 mmu mass tolerance. Only the quantitative results for the unique peptide sequences with the minimum SPS match % of 50 and the average S/N above 10 were considered for the protein quantification. Label free quantification was done in MaxQuant 2.1.3.0 (PMID: 19029910) by searching against Homo sapiens database (Uniprot). The precursor mass tolerance was set to 4.5 ppm and fragment mass tolerance to 20 ppm. Tryptic peptides were accepted with two missed cleavages, variable modifications of methionine oxidation and N-term protein acetylation and fixed cysteine alkylation. FDR threshold for identification was set to 1%. Proteins were quantified by MaxLFQ algorithm (PMID: 24942700).

Mass spectrometry data interpretation

TMT reporter intensities from AGO affinity purification samples were normalized in Perseus ver. 2.0.7.0 (PMID: 27348712) so that medians of log2-ratios between Lamin KO and WT for each cell line were 0. Obtained intensities were log2-transformed, tested by Student's T-test and proteins passing 1,5 fold change and $p<0.075$ were considered as having significantly enhanced interaction with AGO proteins in Lamin A KO. MaxLFQ intensities from Lamin A affinity purification samples were log2-transformed and tested as stated above. Enrichment of Gene Ontology Biological Process terms for significant hits from each cell line was determined by DAVID web-based tool (PMID: 12734009). The interaction network was constructed in Cytoscape ver. 3.8.2 (PMID: 14597658) based on protein-protein interaction data from STRING ver. 11.5 (PMID: 30476243) for significant proteins common for both cell lines and adding AGO2 as IP bait.

RNA sequencing

Total RNA was extracted using Quick-RNA Miniprep Kit. Following, the concentration and quality of the RNA was analyzed using Agilent 2200 TapeStation System. RNA samples with RNA Integrity Number higher than 8 were sent to SNP&SEQ Technology Platform (NGI Uppsala, Sweden). Libraries was prepared from 300 ng RNA using the Illumina Stranded Total RNA library preparation kit, including Ribo-Zero Plus treatment (20040525/20040529, Illumina Inc.) according to manufacturer's instructions. For indexing Unique Dual Indexes (20040553/20040554, Illumina Inc.) were used. Sequencing was carried out with NovaSeq 6000 system using paired-end 150 bp read length, S4 flowcell and v1.5 sequencing chemistry. As a control sequencing library for the phage PhiX was included and a 1% spike-in in the sequencing run. RNAseq data were preprocessed using the RNAseq nf-core pipeline [38]. Differential expression analysis was done using DEseq2 [39], on genes with at least 10 reads in at least 3 samples. Genes with FDR adjusted p-value < 0.01 and absolute log2 fold change > 0.5 were considered differentially expressed. Hypergeometric test, implemented in TopGO, were used to look for enriched Gene Ontology annotation among the differentially expressed genes. The fraction of reads mapping to introns and other genomic regions was calculated using ReSQC [40].

Fluorescent PhotoActivatable Ribonucleoside-enhanced CrossLinking and ImmunoPrecipitation (fPAR-CLIP)

AGO PAR-CLIP was carried out by isolating the proteins using the T6B peptide as mentioned above. Following, fPAR-CLIP library preparation, sequencing and initial data processing was performed as described in [41] with minor modifications. Briefly, to obtain AGO proteins RNA footprints, unprotected RNA was digested on beads with 1 U RNase T1 (EN0541, ThermoFisher) for 15 min at RT. Next, the beads were washed three times with RIPA buffer and three times with dephosphorylation buffer (50 mM Tris–HCl, pH 7.5, 100 mM NaCl, 10 mM $MgCl_2$). After washing, the protein bound RNA was dephosphorylated with Quick CIP (M0525S, New England Biolabs) for 10 min in 37°C. Post dephosphorylation the beads were washed three times with dephosphorylation buffer and three times with PNK/ligation buffer (50 mM Tris-HCl, pH 7.5, 10 mM $MgCl_2$). Following, 0,5 µM fluorescently tagged 3′ adapter (MultiplexDX) were ligated with T4 Rnl2(1–249)K227Q (M0351, New England Biolabs) overnight at 4°C and washed three times with PNK/ligation buffer. Next, RNA footprints were phosphorylated using T4 PNK (NEB, M0201S) for 30 min in 37°C and washed three times in RIPA buffer. To release the proteins the beads were incubated at 95°C for 5 min in 2× SDS Laemmli buffer. Next, the eluates were separated on a 4-12% SDS/PAGE gels (NW04122BOX, Invitrogen) and AGO:RNA complexes visualized on the IR 680 channel (Chemidoc MP system, Bio Rad). Subsequently, appropriate AGO:RNA bands were excised from the gel and protein digested with Proteinase K (RPROTK-RO, Sigma Aldrich) and released RNA isolated via phenol:chlorophorm phase separation. Following, 5′ adapter ligation (MultiplexDX) was performed on the purified RNA samples with 0,5 µM of the adapter and Rnl1 T4 RNA ligase (EL0021, ThermoFisher) for 1 h at 37°C. Next, the RNA was reverse transcribed using SuperScript IV Reverse Transcriptase (18090010, ThermoFisher) according to manufacturer's instructions. The libraries were amplified in a series of PCR reactions performed using Platinum Taq DNA polymerase (10966034, ThermoFisher) and size selected with 3% Pippin Prep (CSD3010, Sage Science). Sequencing of the libraries was carried out on Illumina NovaSeq 6000 platform. For data processing Bcl2fastq (v2.20.0), Cutadapt (cutadapt 1.15 with Python 3.6.4) [42], PARpipe (https://github.com/ohlerlab/PARpipe) and Paralyzer [43] were used. The 3′ and 5′ adaptor sequences and sequencing primers used in the study are listed below.

Oligo name	Sequence
3′ adapter	5′-rAppNNTGACTGTGGAATTCTCGGGT(fl)GCCAAGG-(fl) (MDX-O-226-29.51-2xAF660, Multiplexdx)
5′ adapter	5′(aminolinker-)GTTCAGAGTTCTACAGTCCGACGATCrNrNrNrN (MDX-O-264, Multiplexdx)
RT Primer	GCCTTGGCACCCGAGAATTCCA
5′ short PCR primer	CTTCAGAGTTCTACAGTCCGACGA
5′ long PCR primer	AATGATACGGCGACCACCGAGATCTACACGTTCAGAGTTCTACAGTCCGA
SHSY5Y WT T 3′ Index primer	CAAGCAGAAGACGGCATACGAGATATGGAAGGGTGACTGGAGTTCCTTGGCACCCGAGAATTCCA
SHSY5Y Lamin A KO T 3′ Index primer	CAAGCAGAAGACGGCATACGAGATGTTACGCAGTGACTGGAGTTCCTTGGCACCCGAGAATTCCA
SHSY5Y Lamin A KO C1 3′ Index primer	CAAGCAGAAGACGGCATACGAGATTCGGTTACGTGACTGGAGTTCCTTGGCACCCGAGAATTCCA
SHSY5Y Lamin A KO C2 3′ Index primer	CAAGCAGAAGACGGCATACGAGATATGACGTCGTGACTGGAGTTCCTTGGCACCCGAGAATTCCA
SHSY5Y Lamin A KO C3 3′ Index primer	CAAGCAGAAGACGGCATACGAGATGCTGTAAGGTGACTGGAGTTCCTTGGCACCCGAGAATTCCA
SHSY5Y Lamin A KO N1 3′ Index primer	CAAGCAGAAGACGGCATACGAGATGCAATGGAGTGACTGGAGTTCCTTGGCACCCGAGAATTCCA
SHSY5Y Lamin A KO N2 3′ Index primer	CAAGCAGAAGACGGCATACGAGATATCTCGCTGTGACTGGAGTTCCTTGGCACCCGAGAATTCCA
SHSY5Y Lamin A KO N3 3′ Index primer	CAAGCAGAAGACGGCATACGAGATGGCTATTGGTGACTGGAGTTCCTTGGCACCCGAGAATTCCA

Saracatinib treatment

A375 and SHSY5Y Lamin A KO cells were seeded at a density of 17,000 cells/cm^2. 24 h later cells were treated with 20 µM saracatinib (7189, TOCRIS) or DMSO (D2650, Sigma-Aldrich) for control cells. Cells were harvested after 4 h, lysed and/or fractionated and assessed by western blotting.

Proteosome inhibition assay

A375 and SHSY5Y Lamin A KO cells were seeded at a density of 17,000 cells/cm^2. After 24 h cells were treated with 20 µM saracatinib and 40 µM MG132 (a proteasomal inhibitor) for 4 h. Control cells were treated with DMSO instead of MG132. Following the treatment, cells were lysed and/or fractionated and assessed by western blotting.

Afatinib treatment

A375 and SHSY5Y Lamin A KO cells were seeded at a density of 17,000 cells/cm^2. After 24 h cells were treated with 1 µM afatinib (6812, TOCRIS). Control cells were treated with DMSO. Following a 24 h treatment, cells were subjected to biochemical fractionation and protein expression and localization was assessed by western blotting.

Oxidative stress assessment

For detection of H_2O_2 species in cell culture media of SHSY5Y and A375 Lamin KO and WT cells ROS-Glo™ H_2O_2 Assay (G8820, Promega) was used. Additionally, to trigger intracellular ROS production, cells were treated with 25 µM Menadione (M5625, Sigma Aldrich) for 3 h. Furthermore, ROS quenching was carried out by treating cells with 5 mM N-acetyl cysteine (NAC) (616-91-1, Merck) for 1 h.

EGF treatment

A375 and SHSY5Y WT cells were seeded at a density of 7,000 cells/cm^2. After 24 h cells were treated with 20 ng/ml EGF (PHG0314, Gibco). Cells were harvested after 6 h treatment for A375 cells and 24 h for SHSY5Y cells and then lysed and/or fractionated and assessed by western blot analysis.

RESULTS

The subcellular localization of AGO2 is affected by the nuclear lamina composition

The subcellular localization of RNA binding proteins is relevant to their function. Although, AGO2 is best studied in the cytoplasm [20, 44-45], nuclear AGO2 has also been characterized [17, 20, 45-47] raising questions regarding nuclear RNAi and additional putative functions of AGO2 in the nucleus. To probe AGO2 nuclear localization in cancer cells, we performed biochemical fractionation experiments in twelve different human cell lines, and detected fluctuating levels of AGO2 between the cytoplasmic and nuclear fractions (**Figure 1A-D**). In seven of the screened cell lines, nuclear AGO2 comprised at least 30% and up to 60% of the total AGO2 protein (**Figure 1C,D**), while the other five cell lines express seemingly negligible levels of nuclear AGO2 (**Figure 1B,D**). No pattern was observed in cell origin or cancer stage in the cells expressing nuclear AGO2.

Cytoplasmic:nuclear localization of macromolecules is bridged by the NE. Proteins exceeding a molecular weight of 40 kDa are actively transported through the nuclear pore complexes (NPC), which are a group of various, large multiprotein complexes, embedded in the NE [48]). We hypothesized that the NE restricts nuclear AGO2 translocation and, since the nuclear lamina is a major component of the NE, that the nuclear entry of AGO2 may be promoted by reduced rigidity of the nuclear lamina meshwork. To test the possible effect of Lamin levels on AGO2 subcellular localization we opted for Lamin A/C and Lamin B1 depletion by *LMNA* and *LMNB1* targeting siRNAs (**Supplemental Figure 1A**). A375 and SHSY5Y cell lines were selected because they are characterized by low levels of nuclear AGO2 (**Figure 1B,D**), and their proliferation rate and tumorigenicity differs significantly, with SHSY5Y characterized by slower proliferation (**Figure 1E**) and less tumor formation in mice [49-50]. 48 hours after siRNA transfections (**Supplemental Figure 1A**) we performed a series of biochemical fractionation experiments in the *LMNA* and *LMNB1* siRNA-transfected cells, which revealed that the reduction of Lamin A/C levels triggered AGO2 nuclear translocation in both A375 melanoma and SHSY5Y neuroblastoma cells (**Figure 1F,G**). Targeting Lamin B1, on the other hand, also altered nuclear AGO2 translocation in A375 and SHSY5Y cells, yet it was not as pronounced as with Lamin A/C siRNAs (**Figure 1F,G**).

Taken together, our results indicate that the nuclear lamina composition favors cytoplasmic localization of AGO2 in certain cancer cells, which can be reversed when Lamin A/C levels are diminished.

Knockout of Lamin A affects AGO2 subcellular localization in A375 and SHSY5Y cells

The striking nuclear translocation of AGO2 in A375 and SHSY5Y cells transfected with siRNAs against *LMNA*, prompted us to further explore the correlation between *LMNA* expression and AGO2 subcellular localization. Therefore, we performed CRISPR-Cas9 to KO Lamin A in A375 and SHSY5Y, two cell lines negative for nuclear AGO2, and in HeLa cervical cancer cells, which are positive for nuclear AGO2 (**Figure 1B-D**). We targeted the CRISPR-Cas9 to the constitutive exon 9 of the gene, which is common between Lamin A and Lamin C and indispensable to produce A-type Lamins [51] (**Figure 2A**). After successful integration of both puromycin and G418 resistance cassettes we observed complete KO of Lamin A, while, unexpectedly, low levels of Lamin C were still detectable. The functionality of the expressed form of Lamin C protein was not further evaluated. The Lamin A KO was verified by PCR for the integration of puromycin and G418 resistance cassettes as well as eGFP (**Figure 2B,C, Supplemental Figure 2A**) and by western blotting using either Lamin A/C antibody or antibody specific for Lamin A (**Figure 2D,E**). A series of immunofluorescence experiments were performed in the WT and Lamin A KO A375 and SHSY5Y cells to further confirm Lamin A protein KO and to assess the cellular morphology of the Lamin A KO cells. Consequently, we observed a lack of Lamin A expression in A375 and SHSY5Y KO cells (**Figure 2F,G**). The morphology of A375 cells did not alter significantly upon Lamin A KO, however, the loss of Lamin A resulted in complete atrophy of neurites of SHSY5Y cells (**Supplemental Figure 2B**). Furthermore, the nuclei and cytoplasm of the Lamin A KO cells were misshapen, however, the effect was more visible in the case of SHSY5Y Lamin A KO cells (**Figure 2F,G**). Additionally, we showed that RNA Polymerase II, Histone H3 and Lamin B1 nuclear localization, as well as cytoplasmic-localized Actin, was not affected by Lamin A KO (**Figure 2F,G**), which indicates that the NE is functionally not compromised in the Lamin A KO cells. To further exclude the occurrence of nuclear ruptures and unspecific nuclear translocation of proteins in the Lamin A KO cells, we transfected A375 and SHSY5Y WT and Lamin A KO cells with NLS-GFP constructs. NLS-GFP signal was equally confined to the nucleus in both WT and Lamin A KO cells, with minimal GFP signal observed in the cytoplasm, further pointing to the stability of the NE (**Figure 2H,I**).

As mentioned above, siRNA-mediated silencing of Lamin A/C expression translocated AGO2 into the nucleus (**Figure 1F,G**). To further explore the link between complete knockdown of Lamin A and AGO2 localization, we fractionated A375 and SHSY5Y WT and Lamin A KO cells (**Figure 2J,K**), as well as HeLa WT and Lamin A KO cells (**Supplemental Figure 2C**).

Fractionation experiments showed predominantly cytoplasmic localization of AGO2 protein in A375 and SHSY5Y WT cells (**Figure 2J,K**). However, potent, and significant, upregulation of nuclear AGO2 expression was found in both A375 and SHSY5Y Lamin KO cells (**Figure 2J,K**). A similar trend was observed for the remaining AGO family proteins in both A375 and SHSY5Y Lamin KO cells (**Supplemental Figure 2C,D**). Subcellular localization of AGO2 protein was additionally assessed in HeLa Lamin A KO cells. Since HeLa cells are characterized by ubiquitous distribution of AGO2 between the nucleus and the cytoplasm (**Figure 1C,D**), Lamin A KO minimally affected AGO2 localization (**Supplemental Figure 2E**). Additionally, we characterized AGO2 protein and RNA expression levels upon Lamin A KO. We observed no significant change in *AGO2* mRNA levels in A375 cells (**Supplemental Figure 2F**). In contrast, *AGO2* mRNA levels was significantly increased in SHSY5Y Lamin A KO cells (**Supplemental Figure 2G**). This trend was also reflected in AGO2 protein levels (**Supplemental Figure 2H,I**).

To test if rescuing Lamin A/C expression is sufficient to restore the WT cellular phenotype of A375 and SHSY5Y cells, where nuclear AGO2 is not expressed, we performed *LMNA* overexpression experiments in the Lamin A KO cells. Normal localization of ectopically expressed Lamin A/C at the nuclear envelope was confirmed by immunofluorescent staining using anti-Lamin A antibodies, and the levels of the plasmid uptake was assessed by GFP expression (**Figure 2L,M**). Moreover, the levels of Lamin A/C ectopic expression were confirmed by western blot (**Figure 2N,O**). Biochemical fractionation experiments revealed a significant decrease in nuclear AGO2 content in *LMNA* overexpressing cells in both A375 and SHSY5Y Lamin A KO cells, resulting in a rescue of WT phenotype, where AGO2 has a predominant cytoplasmic distribution (**Figure 2P,Q**). This indicates that nuclear import of AGO2 is directly linked with diminished levels of Lamin A.

RNA sequencing analysis of Lamin A KO cells reveals a global downregulation of gene expression which is amplified in SHSY5Y cells

To assess the changes in gene expression between A375 and SHSY5Y Lamin A KO cells compared to their WT counterparts, we performed RNA sequencing experiments. Principal Component Analysis (PCA) revealed significant differential gene expression changes between the Lamin A KO and WT cells (**Supplemental Figure 3A,B**). In A375 we observed 1020 upregulated genes and 1582 downregulated genes (**Figure 3A,B**). In SHSY5Y we found 1479 upregulated genes and 4067 downregulated genes (**Figure 3A,B**). The top 30 up- and

downregulated genes, with regards to p-value, were also plotted as a heatmap (**Figure 3C**) and a GO pathway analysis was performed for the top 100 differentially expressed genes (**Supplemental Figure 3C**).

To understand, in detail, the biological processes that are affected, as a consequence of the loss of Lamin A, we next performed gene set enrichment analysis (GSEA), allowing for the comparison between our RNAseq data and available resources [53-53]. The analysis revealed many significantly enriched pathways. Of note, the differential gene expression between Lamin A KO vs WT SHSY5Y cells revealed a significant positive correlation with gene-sets involving the EGFR signaling pathway, MYC targeting genes, as well as with E2F pathway and G2M genes controlling the cell cycle (**Figure 3D**). In the case of A375 cells, we did not find any significant, positively correlated, gene-sets. However, several pathways were downregulated in both A375 and SHSY5Y cells including those controlling cell death, the NOTCH signaling pathway, IL6-JAK-STAT3 and genes controlling the epithelial-mesenchymal transition (EMT) (**Figure 3D**).

Our observations collectively suggest different mechanisms of gene regulation in the A375 and SHSY5Y cells to cope for the loss of Lamin A, however, both mechanisms lead to a potent accumulation of AGO2 in the nucleus. The nuclear translocation of AGO2 may therefore be regulated by different cellular mechanisms depending on the cancer cell type.

RNAi activity is significantly diminished upon Lamin A KO

Having determined that there is substantial translocation of AGO2 into the nucleus in cancer cells when Lamin A levels are diminished, we aimed at understanding the putative functions of AGO2 in the nucleus. AGO2, guided by miRNAs, mediates gene regulation in the cytoplasm by targeting mRNAs predominantly within coding regions and 3′ untranslated (3′UTR) regions [12]. Previous studies provided evidence that natural cell conditions, such as viral infection [54] or early differentiation [20], comprise functional AGO2 nuclear regulation and that AGO2 preferentially binds 3′UTRs and introns within pre-mRNAs [20]. To gain detailed information on AGO-dependent regulation on gene expression in Lamin A KO cells we focused on SHSY5Y cells and performed fPAR-CLIP [41]. fPAR-CLIP of AGO proteins was conducted from total cell lysate in SHSY5Y WT and Lamin A KO cells, as well as from three biological replicates of cytoplasmic and nuclear fractions of SHSY5Y Lamin A KO cells. Since all three replicates showed high correlation (>85%), all further analysis was done on one representative fPAR-CLIP sample

(**Supplemental Figure 4A**). In total cell fraction of WT cells AGO binding was identified at 59,257 sites, while in Lamin A KO cells 37,370 sites were mapped. Then, in AGO fPAR-CLIP from nuclear and cytoplasmic fractions of SHSY5Y Lamin A KO cells an average of 39,439 cytoplasmic and 47,740 nuclear binding sites were mapped (**Supplemental Figure 4B, Supplemental Table 1**). Moreover, between 500,000 and 1,500,000 crosslinked reads were found for each library (**Supplemental Figure 4C**). These binding sites distributed over 9300 genes in WT cells, 7217 genes in Lamin A KO cells, 7601 genes in the cytoplasm and 8184 genes in the nucleus of Lamin A KO cells (**Supplemental Table 1**).

As expected, AGO fPAR-CLIP using total SHSY5Y WT cell lysates revealed gene occupancy predominantly at 3'UTRs (**Figure 4A**). However, upon Lamin A KO we observed a less specific occupancy of the AGOs, which more evenly distributed to 3'UTR, introns, and coding regions (**Figure 4B**), reflecting the shift in AGO subcellular localization. However, to our surprise, nuclear and cytoplasmic AGOs were not distinct in their target RNAs occupancy, where also cytoplasmic AGO proteins targeted introns (**Figure 4C,D**). Cytoplasmic prevalence of RNA introns cannot be explained by a general increase in intronic transcripts, as a consequence of Lamin A loss, which was revealed by RNAseq (**Supplemental Figure 4D**).

Lamin A KO triggered a massive shift in gene expression, with most genes downregulated upon Lamin A KO (**Figure 3A,B**). To investigate the role of AGO proteins in this phenomenon, we calculated the expression change of all genes upon Lamin A KO and tested if AGO targets correspond to the same genes that undergo downregulation. Firstly, we ranked genes by their AGO occupancy in WT cells and used cumulative distribution analysis to test the effect of Lamin A KO on their expression level (**Figure 4E**). The analysis revealed that specifically AGO targets in WT cells are increasingly downregulated in response to Lamin A KO, and directly proportional to the binding strength of AGO (**Figure 4E**). Unlike AGO targets in WT cells, the targets acquired by AGO in Lamin A KO cells, were generally not among the genes that were downregulated in response to the KO of Lamin A (**Figure 4F**). Excluding the top 5% of AGO bound transcripts that were slightly downregulated, most of AGO targets in these cells were not downregulated in Lamin A KO cells, even relative to non AGO targets (**Figure 4F**). Noteworthy that even for the top 5% of targets, the extent of downregulation for

AGO targets in WT cells is about 60% more than for AGO targets in Lamin A KO cells (**Figures 4E,F**).

When specifically comparing the top 5% of binding targets in WT vs Lamin A KO we found that the transcript occupancy drastically changes (**Figure 4G**). In WT cells the top 5% binders align predominantly to 3' UTRs, while in Lamin A KO cells AGO binding was mapped preferentially to intronic sites (**Figure 4G**). Based on this, we assessed the overlap between top 5% AGO targets in WT and Lamin A KO cells, and as shown, of roughly 465 genes in WT and 360 genes in Lamin A KO cells 77 genes were top AGO targets in both cell lines (**Figure 4H**). GO analysis of the subset of genes which are unique to AGO occupancy in either WT or Lamin A KO cells, indicate predominant involvement in positive regulation of cell division and miRNA-mediated translational repression or regulation of transcription processes, respectively (**Supplemental Figure 4E,F**). Furthermore, the best transcripts bound to AGO in either WT or Lamin A KO cells were ranked (**Supplemental Figure 3G,H**). Top AGO targets include RORA in WT cells and MAP7D2 in Lamin A KO cells.

In an effort to gain even higher resolution of AGO interactions with mRNAs upon Lamin A KO and the newly acquired nuclear localization, we performed fPAR-CLIP in cytoplasmic and nuclear fractions of Lamin A KO SHSY5Y cells. As described above, we observed similar binding preferences of AGO proteins to functional RNA elements between cytoplasmic and nuclear fractions, including suprising interactions of cytoplasmic AGO with intronic elements (**Figure 4C,D**). As was observed for AGO targets obtained by fPAR-CLIP of total Lamin A KO cells, also when fPAR-CLIP followed cell fractionation AGO associated transcripts generally did not correspond to the large set of genes downregulated as a result of Lamin A KO (**Figures 4I,J**). However, while similarly only the top 5% of AGO targets post fractionation were downregulated in the Lamin A KO cells, the magnitude of the measured affect was higher (**Figure 4I,J**). We observed high overlap between AGO targeted transcripts in the cytoplasmic and nuclear fractions (**Figure 4K**), which points to a lack of preferential binding to targets in either of the fractions upon Lamin A KO. Nevertheless, we identified 1393 exclusively-nuclear targets of AGO (**Figure 4K**). Cumulative distribution of these transcripts showed that approximately 20% of the exclusively nuclear AGO targets are destabilized (**Figure 4L**).

Interestingly, GO analysis of top 5% AGO targets revealed involvement in Wnt pathway (**Supplemental Figure 4I**).

For assessment of miRNAs loaded into AGO proteins, we crossed the genomic coordinates of AGO binding sites along mRNAs with those of annotated miRNA target sites. Of several discrepancies between the miRNA species guiding AGO proteins in WT and Lamin A KO cells, reduced binding to miR-27A target sites in Lamin A KO was the most striking one, accompanied by an increase in binding to miR-27B and miR-320A target sites (**Figure 4M**). However, the distribution of AGO loaded miRNAs between the cytoplasm and nucleus was similar, and reflected the general trend of AGO occupancy in Lamin A KO cells with no significant miRNA preference in either of the fractions (**Supplemental Figure 4J**)

Taken together, Lamin A KO resulted in a general trend of mRNA downregulation accompanied by nuclear translocation of AGO. Our analysis of AGO-dependent gene regulation in Lamin A KO vs WT cells revealed that the pool of AGO2 which translocate into the nucleus does not predominantly engage in gene regulation. In these conditions, the function of the remaining cytoplasmic AGO2 is probably compromised and seems to only regulate the top fifth percentile of its targets (**Figure 4F,I,J**). Lamin A KO yields a prominent suppressive gene regulatory effect which may mask the RNAi potential of nuclear AGOs.

Loss of Lamin A promotes AGO2 interaction with FAM120A, nucleoporins and chromatin regulators

To gain more insights into the nuclear functions of AGO1-4, we investigated the interactome of nuclear AGO proteins by mass spectrometry using the T6B peptide, which unbiasedly binds all four AGO proteins [36]. We identified 184 AGO interactors enriched in the A375 Lamin A KO nuclei, compared to WT nuclei, which do not express nuclear AGO and therefore are treated as a negative control (**Figure 5A, Supplemental Table 2**). Respectively, in the SHSY5Y Lamin A KO nuclei, compared to WT nuclei, we identified 141 AGO interacting partners (**Figure 5B, Supplemental Table 2**). Gene ontology (GO) analysis of the nuclear interacting proteins revealed that they are predominantly involved in various aspects of RNA processing (**Supplemental Figure 5A,B**).

Further examination of the enriched interacting partners of nuclear AGO revealed that there are 20 protein interactors which overlapped between A375 and SHSY5Y cells (**Figure 5C**). Functional annotation analysis of this subset of interacting partners further confirmed that

they are involved in regulation of various aspects of RNA processing (**Figure 5D**). The list also included nuclear pore complex (NPC) components Nup85, Nup88 (**Supplemental Table 2**) and 4 DNA associated regulators, including Histone H2B, H2A.V, and the transcription initiation factor TFIID (**Figure 5D**). Interestingly we also identified the Constitutive coactivator of PPAR-gamma-like protein 1, FAM120A, as an interacting partner of AGO in the nucleus. FAM120A is a RNA binding protein involved in the activation of Src kinase upon oxidative stress [55]. FAM120A has previously been suggested to interact with AGO2 [13,56], and we further validated this hit by performing co-immunoprecipitation assay between AGO2 and FAM120A (**Figure 5E,F**). In both A375 and SHSY5Y cells, AGO2:FAM120A interaction occurred in Lamin A KO cells, but not in WT cells (**Figure 5E,F**).

Further exploring the proteomics data from the individual cell lines revealed that AGO2 may interact with Nup85, Nup88 and Nup205 in A375, as well as Nup85, Nup88, Nup210, Nup214 and Nup155 in SHSY5Y (**Figure 4G**). Nup proteins are crucial components of the NPC complexes, driving the regulation of cytoplasmic:nuclear transport [48]. Therefore, we performed siRNA experiments against Nup85 (**Supplemental Figure 5C**), common between A375 and SHSY5Y, and measured the nuclear localization of AGO2 by biochemical fractionation assays. We observed a reduction of nuclear localized AGO2 in response to silencing Nup85 in SHSY5Y cells (**Figure 5H**).

The shift towards nuclear localization together with the identification of AGOs in complex with nucleoporins prompted us to evaluate the proximitome of the NPC using proximity labeling procedures [57]. Proximity labeling and subsequent purification allows for stringent purification of proteins from specific subcellular localizations, without biochemically fractionating cells. Therefore, we established SENP2-APEX2 expressing A375 WT and Lamin KO cells. The correct localization of SENP2-APEX2 was visualized to the NPC (**Figure 5I, Supplemental Figure 5D**). Further, we verified that V5-tagged SENP2-APEX2 protein was expressed (**Supplemental Figure 5E**). By performing co-immunoprecipitation assay between Streptavidin and AGO2 we observed an enriched proximal localization of AGO2 to the NPC in the Lamin A KO cells, compared to WT cells (**Figure 5J**).

Additionally, we speculated that AGO2 may interact with Lamin A in Hela cells, which are normally positive for nuclear AGO2 (**Figure 1C**). Indeed, we found that AGO2 is in complex with Lamin A and this interaction is lost in Lamin A KO cells (**Supplemental Figure 5F**). Moreover, we analyzed Lamin A interactome by mass spectrometry in A375 WT and Lamin A

KO cells to find possible indications of pathways that may be altered upon loss of Lamin (**Supplemental Table 2**). The GO analysis of Lamin A interacting partners revealed involvement in DNA replication and cell division processes (**Supplemental Figure 5G**), which is in line with the observed phenotype of Lamin A KO cells.

Decrease in Lamin A levels is mirrored in cancer progression and cellular migration, contributing to cancer aggressiveness [58]. In this condition, the sum of our findings indicates that a portion of AGO2 redistributes to the nucleus, where it interacts with RNA processing factors, possibly facilitating the cancer phenotype.

Oxidative stress in Lamin A KO cells activates FAM120A and Src kinase which leads to an interaction with AGO2 in the nucleus

FAM120A has been found to be activated in response to oxidative stress [55]. As this protein was identified to interact with nuclear AGO2 in both A375 and SHSY5Y cells, we questioned if the loss of Lamin A causes increase in oxidative stress response. We measured the levels of hydrogen peroxide (H_2O_2) in WT vs Lamin A KO cells at steady state levels but also in response to Menadione, an agent which induces oxidative stress (**Supplemental Figure 6A,B**). The specificity of Menadione was further validated by using N-acetyl L cysteine (NAC), a specific inhibitor of oxidative stress. We observed an increase in H_2O_2 levels in Lamin A KO cells, which was further highlighted upon the addition of Menadione (**Figure 6A,B Supplemental Figure 6A,B**), indicating that the Lamin A KO cells are more sensitive to oxidative stress response. In line with this type of investigation, we also measured cell viability (**Supplemental Figure 6C,D**) cell proliferation (**Supplemental Figure 6E,F**) and cell cycle rate (**Supplemental Figure 6G,H**) in WT vs Lamin A KO cells. Cell viability and cell proliferation were significantly increased after Lamin A KO, with enriched in G2/M phase of the cell cycle (**Supplemental Figure 6G,H**) .

A feature of FAM120A activation, upon oxidative stress, is its ability to trigger signal transduction, specifically by interacting with and activating the Src kinase [55]. Src has been shown to interact with and phosphorylate AGO2 at three specific phosphorylation sites - Y393, Y529 and Y749 [24]. Even though the mass spectrometry (**Figure 5A,B**; **Supplemental Table 2**) did not detect an interaction between AGO2 and Src, we were nevertheless able to identify an interaction in Lamin A KO SHSY5Y cells (**Figure 6D**), but not in A375 (**Figure 6C**), by performing co-immunoprecipitation assay. Interestingly, AGO2 interacted with pan-Src, active (site Y419) and inactive (site Y530) Src forms (**Figure 6D).** Similarly to AGO2:FAM120A

interaction (**Figure 5E,F**), AGO2:Src interaction was enriched in Lamin A KO cells as compared to WT cells (**Figure 6D**).

Having shown that AGO2 interacts with Src upon Lamin A KO, we further sought to characterize the FAM120A-Src-AGO2 axis by investigating the total levels of FAM120A, pan-Src, as well as the active and inactive forms of Src and its upstream activator EGFR (**Figure 6E,F**). FAM120A protein and active Src form was significantly upregulated in both A375 and SHSY5Y Lamin A KO cells vs WT cells, while the total levels of inactive and total Src did not change significantly between the two cell lines (**Figure 6E,F**). Likewise, the epidermal growth factor receptor (EGFR), an upstream receptor in the Src signaling pathway, which is known to be activated by oxidative stress, was also upregulated in Lamin A KO cells, particularly evident by probing against the active from of EGFR at Y1068 (**Figure 6E,F**). Next, we investigated the subcellular localization of these proteins. FAM120A and Src follows AGO2 localization, and are, hence, exclusively cytoplasmic in WT cells, but localize ubiquitously upon Lamin A KO (**Figure 6G,H, Supplemental Figure 6I,J**). However, both phosphorylated Src species localized preferentially to the nucleus of the Lamin A KO cells (**Figure 6G,H, Supplemental Figure 6I,J**).

Since FAM120A localizes ubiquitously in Lamin A KO cells, whilst the phosphorylated species of Src localized preferentially to the nucleus, we wanted to get detailed information on where AGO2 interacts with FAM120A in the cell. Biochemical fractionation assay, in conjunction with T6B immunoprecipitation assay, revealed that in both A375 and SHSY5Y, AGO2 and FAM120A interact exclusively in the nucleus (**Figure 6I,J**).

Taken together, our observations indicate that upon Lamin A KO, cells are more prone to oxidative stress, which activates a signaling cascade downstream of at least EGFR. Phosphorylated species of Src and FAM120A interact with AGO2 in the nucleus. These interactions could play an important role in the regulation of the nuclear translocation or the stability of AGO2 since posttranslational modifications can re-localize and/or stabilize proteins.

Activated Src and EGFR regulates the cytoplasmic turnover of AGO2

AGO2 activity has been found to be regulated by oncogenic kinases [23-24]. Both Src and EGFR are known to phosphorylate AGO2 [23-24]. We also confirmed that AGO2 and EGFR interact in Lamin A KO cells by performing an co-immunoprecipitation assay (**Figure 6K**,**L**). Therefore, we wondered what effect EGFR/Src pathway activation might have on AGO2 levels and subcellular localization. To investigate this phenomenon, we treated Lamin A KO cells with

saracatinib, a potent drug that specifically targets Src kinase [59] (**Supplemental Figure 7A,B**). We found that AGO2 levels are reduced in total cell lysate upon Src inhibition (**Figure 7A,B**), indicating that Src may have a stabilizing effect on AGO2 protein. To test this, we treated cells with the proteasomal inhibitor MG132, in conjunction with saracatinib treatment. Under these conditions, we found that AGO2 protein levels can indeed be rescued by inhibiting the proteosome (**Figure 7C,D**). Next, we performed biochemical fractionation assay, after inhibiting Src activity, to investigate if the inactivation of Src could affect subcellular localization of AGO2 in the Lamin A KO cells. Surprisingly, we found that the total levels of AGO2 reduction is actually due to the depletion of AGO2 levels specially in the cytoplasm (**Figure 7E,F**).

Src is activated by both FAM120A and EGFR. To test if we see a similar phenotype of decreased AGO2 protein levels in the cytoplasm, as a consequence of blocking EGFR, we treated cells with the selective EGFR inhibitor - afatininb [60]. Like with saracatinib treatment we found that total AGO2 levels decrease specifically in the cytoplasm (**Figure 7G**) in A375 Lamin A KO cells. However, no changes in AGO2 cytoplasmic or nuclear levels were observed after afatinib treatment in SHSY5Y Lamin A KO cells (**Supplemental Figure 7C**).

Having established that nuclear accumulation of AGO2, upon Lamin A KO, is linked with FAM120A, Src and EGFR activation by oxidative stress we next asked if the phenomenon could be recapitulated in WT cells. To address this question, we induced oxidative stress, overexpressed Src kinase or activated EGFR by treating cells with epidermal growth factor (EGF). Firstly, we induced oxidative stress by treating WT cells with Menadione for 3 h (**Supplemental Figure 6A,B**). Biochemical fractionation of the control vs treated cells revealed that AGO2 did not shift localization upon Menadione-mediated oxidative stress (**Supplemental Figure 7D,E**). Similarly, overexpression of Src kinase, regardless of its activity, did not influence AGO2 subcellular localization (**Supplemental Figure 7F,G**). Nevertheless, we found that treatment with 20 ng/ml of EGF for 6 h triggered AGO2 into the nucleus in A375 WT cells (**Figure 7H**). Moreover, AGO2 translocation was accompanied by potent Src kinase activation (**Figure 7H**). However, in the case of SHSY5Y cells no effect was observed after treatment with EGF (**Supplemental Figure 7H**). Of note, active Src was predominantly detected in the cytoplasm of A375 and SHSY5Y WT cells (**Figure 7H; Supplemental Figure**

7H) in contrast to exclusively nuclear localization of active Src kinase in Lamin A KO cells (**Figure 6G,H; Supplemental Figure 6I,J**).

EGFR has previously been found to negatively regulate the RNAi activity of AGO2 by phosphorylating AGO2 at Y393 [23]. Our own findings indicates that upon EGFR or Src kinase inhibition, the cytoplasmic AGO2 levels are downregulated, while the nuclear levels are stable. In line with these observations, we reasoned that, in the nucleus, AGO2 could be phosphorylated and that it is the phosphorylated species of AGO2 which interacts with FAM120A. We performed a String network analysis on our proteomics data (**Figure 7I**), which suggested that AGO2 is in complex with FAM120A and TNRC6A via the poly(A) binding protein PABPC1. PABPC1 is a nuclear-cytoplasmic shuttling protein and binds 3'poly(A) tail of mRNAs, which favors poly(A) shortening and ultimately leads to mRNA decay [61].

To address our postulations, we firstly investigated the total levels of TNRC6A and PABPC in Lamin A KO vs WT cells (**Figure 7J,K**). We found no differences in PABPC levels in A375 cells **(Figure 7J)**, however, in SHSY5Y cells PABPC was strikingly upregulated upon Lamin A KO (**Figure 7K**). TNRC6A was downregulated in Lamin A KO A375 cells **(Figure 7J)**. On the contrary, in SHSY5Y Lamin A KO cells, we observed upregulation of TNRC6A levels as compared to WT cells **(Figure 7K)**. Following, subcellular localization of PABPC and TNRC6A was measured. We observed that PABPC is ubiquitously distributed in WT and Lamin A KO A375 cells **(Figure 7L)**. A similar trend was observed for SHSY5Y WT cells, while in SHSY5Y Lamin A KO cells the protein was exclusively nuclear (**Figure 7M**). Next, we performed co-immunoprecipitation assays between pAGO2, PABPC, FAM120A and TNRC6A from cytoplasmic and nuclear lysates of Lamin A KO cells. We did not observe an interaction between pAGO2 and PABPC, FAM120A or TNRC6A in A375 Lamin A KO cells **(Figure 7N).** However, in SHSY5Y Lamin A KO cells, pAGO2 interacts with PABPC, FAM120A and TNRC6A only in the nucleus (**Figure 7O**). To test if AGO2 interacts with FAM120A exclusively when AGO2 is phosphorylated at Y393, we transiently expressed Flag-tagged Y393A-AGO2 or WT-AGO2 in SHSY5Y and A375 Lamin A KO cells. Subsequently, we performed a Flag immunoprecipitation between both AGO2 constructs and FAM120A. The expreiments revealed an interaction between FAM120A and both forms of AGO2 protein, in both A375 and SHSY5Y

Lamin A KO cells (**Figure 7P,Q**), indicating that AGO2 phosphorylation at Y393 is dispensable for FAM120A interaction.

Lamin A KO causes cellular stress resembling oxidative stress and triggers potent changes in gene regulation. A striking phenotype is further illustrated by the nuclear translocation of AGO2. Our collective data suggest that the loss of Lamin A induces the activation of signaling pathways which robustly regulates AGO2 stability and activity**.**

DISCUSSION

Since the discovery of RNAi, the prevalent view has been that RNAi processes are executed in the cytoplasm. RNAi-mediated silencing of nuclear transcripts was described as significantly harder to achieve as compared to cytoplasmic RNAs [15-16]. Moreover, immunofluorescent-based imaging assays repeatedly showed cytoplasmic AGO2 localization, with enrichment in P-bodies and endoplasmic reticulum [62-63]. However, improved biochemical fractionation techniques and imaging assays convincingly showed the nuclear presence of both AGO2 protein and small RNAs [31-32,64]. AGO2:miRNA complexes actively shuttle to the nucleus [17] and the nuclear localization of AGO2 has been shown in several cell lines, including HeLa and MCF7 used in our study (**Figure 1C,D**) [17,45-47] and embryonic stem cells [20]. On the contrary, in other cancer cells AGO2 localization is predominantly cytoplasmic (**Figure 1B,D**) [20,44-45], suggesting that the fluctuations of nuclear AGO2 is tightly regulated. Yet, the mechanisms regulating the nuclear localization of AGO2, or its mode of entry, remains largely unknown.

The nuclear translocation of AGO2 protein (approx.. 100 kDa) should be transported through the NPC embedded in NE [48]. Since NPCs are also tethered to the cytoskeleton, they provide another platform for cytoplasmic and nuclear crosstalk [66]. Proximity labeling in Lamin A KO cells, when AGO2 translocates into the nucleus, showed that AGO2 is enriched in the NPC proximity (**Figure 5J**). Moreover we observed AGO interaction with different nucleoporins (NUP), which are core NPC components (**Figure 5A,B,G**) and silencing Nup85 in Lamin A KO cells resulted in nuclear exclusion of AGO2 (**Figure 5H**) therefore, our data points to an involvement of Nup85 in selective transport of AGO2 into the nucleus. Since little is known about the mechanisms of AGO2 nuclear entry, our results reveal an intriguing starting point for blocking AGO2 nuclear influx.

The NE composition is highly dynamic in cancer cells. Further, the levels of Lamin A/C are important in mechanosensing, where the levels are inversely related to cell fluidity. During cancer metastasis, the stiffness of the cell decreases, thereby imparting increased mobility [65]. Moreover, Lamins are speculated to play a role in cancer progression and to be altered in response to it [67]. *LMNA* is either mutated or is significantly decreased in breast cancer, ovarian cancer, primary gastric carcinoma and colon cancer [65]. Consistent with reports pointing to tumor-promoting functions of decreased A-type Lamins, our experiments showed

increased viability and proliferation of A375 and SHSY5Y cancer cells in response to Lamin A KO (**Supplemental Figure 6C-H**).

Apart from involvement in cancer onset and metastasis, Lamins are known to play an important role in stem cell differentiation. While B-type Lamins are steadily expressed, Lamin A/C is expressed at very low levels in stem cells, but increases during differentiation [68-69]. High levels of nuclear AGO2 have been shown in mouse and human stem cells [20]. Similarly, our data suggests a negative correlation between nuclear AGO2 localization and Lamin A/C expression (**Figure 1F,G; Figure 2J,K,P,Q**) when silencing Lamin A expression leads to an accumulation of nuclear AGO2 in the two cancer cell lines studied herein, which normally do not express endogenous AGO2 in the nucleus.

The nuclear function of AGO2 in stem cells have been documented [20,70-71]. For instance, AGO2 in the nucleus was required for adipose tissue-derived stem cells survival in response to reactive oxygen species-mediated senescence [70]. Moreover, nuclear levels of AGO2 were higher in primary myoblasts compared to differentiated myocytes [20]. Thus, high nuclear AGO2 may be another factor characteristic of pluripotent stem cells, apart from the well-documented low Lamin A/C expression [68].

The involvement of the nuclear lamina in the regulation of human AGO protein expression and function has not been demonstrated before. Given the crucial role of both protein families in homeostasis and maintenance of cellular identity, the existence of an interplay between Lamin and AGO protein pathways seem inevitable. In this study, we found a relationship between Lamin levels and AGO2 subcellular localization in cancer cells. Different experimental approaches pointed to a potent translocation of AGO2 into the nucleus in SHSY5Y neuroblastoma and A375 melanoma cells upon loss of LMNA expression (**Figure 1F,G; Figure 2J,K**). The nuclear translocation was completely reversed when Lamin A expression was transiently rescued (**Figure 2P,Q**). Thus, nuclear AGO2 expression, in the studied cell lines, seems to be directly dependent on the low A-type Lamins levels.

AGO2 activity is fine-tuned by intracellular kinases. Several of these are also implicated in cancer and uncontrolled proliferation [21]. For instance, in hypoxia, AGO2 is phosphorylated by EGFR kinase at Y393, which attenuates AGO2:DICER binding, resulting in the inhibition of miRNA maturation and subsequently RNAi efficiency [23]. Further, a stabilizing effect of AGO2 phosphorylation by EGFR and MAPK was described [72-73]. AGO2 phosphorylation at residues S824–S834 negatively affects RISC:target RNA interaction; this is

catalyzed by CSNK1A1 kinase, an implicated oncoprotein in leukaemia [74]. Mitogenic AKT3 kinase phosphorylates AGO2 protein at S387, regulating both AGO2 ribonucleolytic activity and localization [25-26]. Furthermore, a recent report documents the phosphorylation of AGO2 by the oncogenic kinase Src at Y393, Y529 and Y749 [24]. Src-mediated AGO2 phosphorylation positively regulated both cell proliferation and migration [24].

Interestingly, upon Lamin A KO we observed upregulation of EGFR and Src kinases activation, (**Figure 6E-H**). Of note, the localization of phosphorylated Src species mimicked AGO2 localization (**Figure 6G,H**), and phosphorylated EGFR levels were increased **(Figure 6E,F)**, suggesting a common regulation of Src and AGO2 subcellular localization. Interestingly, we could point out a decrease in mature miR-27A loading to AGO proteins. Previously, Shen and collegues observed that, upon EGFR downregulation there was an increase in miR-27A maturation in hypoxic conditions [23]. Therefore, the observed decrease in miR-27A among AGO interacting RNAs upon Lamin A KO, seems to be directed by the activation of EGFR kinase. Moreover, inhibition of Src and EGFR kinases by selective small molecule inhibitors saracatinib and afatinib, respectively, resulted in decreased AGO2 stability in the cytoplasm. Specifically, for saracatinib treatment, we observed that the turnover of cytoplasmic AGO2 was via increased proteasomal degradation (**Figure 7A-D**). Interestingly, the nuclear levels of AGO2 remained stable (**Figure 7E,F**). These results stress the importance of intracellular signaling pathways that regulate AGO2 expression, activity, and subcellular localization.

It has been reported that the re-localization of AGO2 and small RNAs to the nucleus occurs in differentiated cells in response to different external stimuli. For instance, treatment of HeLa and HEK293 cells with Arsenic Trioxide, a compound that induces oxidative stress, stimulates AGO2 and small RNAs translocation into nucleus [75]. Yet, oxidative stress by Menadione was not potent enough to influence a shift in localization of AGO2 in A375 and SHSY5Y WT cells (**Supplemental Figure 7D,E**). Moreover, induction of cellular senescence with Interferon γ and Tumor Necrosis Factor resulted in almost exclusive accumulation of AGO2 to the nucleus of MCF7 cells [45]. In the present study, we found that stimulating WT A375 cells with EGF was sufficient to translocate AGO2 to the nucleus (**Figure 7H**). However, overexpression of Src did not affect the subcellular localization of AGO2 (**Supplemental Figure 7F,G)**

Herein, we sought to unravel the mechanism of cytoplasmic-nuclear crosstalk tuned by the nuclear lamina and its effect on nuclear RNAi. Therefore, we generated a Lamin A

knockout system to stringently study AGO2 localization. The loss of Lamin A led to an amplified down regulation of gene expression (**Figure 3A-C**). This effect was particularly evident in SHSY5Y cells (**Figure 3A-C**). The loss of Lamins generally leads to decreased cellular stiffness and increased cell migration, pivotal for cancer cell growth. Therefore, we hypothesized a larger effect of Lamin A KO on SHSY5Y cells as compared to A375 cells since SHSY5Y are less aggressive cancer cells when compared to A375 (**Figure 1E**) [49-50]. Indeed, SHSY5Y amplified its cancer phenotype by acquiring significantly higher cell growth potential (**Supplemental Figure 6C-H**) and loss of neurites pointing to undifferentiation (**Supplemental Figure 2B**), whilst in A375, the loss of Lamin A simply maintains the aggressive status.

Upon the loss of Lamin A, nearly half the pool of cellular AGO2 translocates to the nucleus and to understand if there is a gain of nuclear gene regulatory functions, we performed fPAR-CLIP. We observed a degree of gene regulation in the KO cells, but this was surprisingly much less compared to WT cells (**Figure 4E,F and I,J**). Recently, it was shown that FAM120A and AGO2 interact in stem cells and breast cancer T47D cells [13,55]. Of note, both studies used Flag-AGO2 overexpression systems [13,55]. In our study, we detected an interaction of endogenous AGO2 and FAM120A proteins upon Lamin A KO (**Figure 5E,F**). Additionally, we mapped the AGO2:FAM120A interaction exclusively in the nucleus (**Figure 6I,J**). iCLIP assays of FAM120A and AGO2 in stem cells revealed a fraction of mRNAs that was bound by AGO2 and FAM120A simultaneously [13]. On those subsets of genes, AGO2 did not mediate target degradation [13]. The authors suggested that AGO2 may exist in multiple protein complexes with different functions depending on the specific complex. Indeed, we postulate that FAM120A may have similar mode of action in the Lamin A KO cells and block the RNAi effect of nuclear AGO proteins. Furthermore, we found that FAM120A interacts with phosphorylated AGO2 at Y393. This phosphorylation, mediated by EGFR, is another layer of negative regulation of RNAi function. Taken together, our data supports a predominant inactivation of RNAi function supported by the evidence that FAM120A-AGO2 interact. Moreover, we did not identify canonical RISC protein interactors from the mass spectrometry analysis of AGO proteins purified from the nuclear fraction (**Figure 5D**). For future studies, performing FAM120A fPAR-CLIP in the WT and Lamin A KO backgrounds will further elucidate the relationship between FAM120A:AGO2 nuclear interaction and the effect on bound RNA expression.

In this study we revealed a new layer of regulation of nuclear AGO2. We uncovered that Lamin A downregulation in cancer cells, an alteration promoting cancer aggressiveness, is sufficient to trigger AGO2 nuclear influx. We showed that the NPC complex composition, especially Nup85 protein is important for active transport of AGO2 from the cytoplasm into the nucleus. In the nucleus, we uncovered a potent gene regulation of the top 5% of AGO2 targets. For the remaining targets of AGO2 there was a negligible effect on gene repression. In contrast, potent nuclear RNAi was observed in mESC, where nuclear AGO2 is expressed at high levels in steady state conditions [20]. These contradictory observations may imply that the function of nuclear AGO2 translocation under stress is to rapidly inhibit RNAi – similarly to well described stress granules formation upon external stimuli [76]. Additionally, our data corroborate and complement an already documented link between AGO2 and EGFR/Src kinases [23-24,72-73]. Interestingly, inhibition of Src and EGFR kinases only affected levels of cytoplasmic AGO2, further suggesting that the nuclear pool of AGO2 is mostly inactive for gene silencing.

DATA AVAILABILITY

The mass spectrometry proteomics data have been deposited to the ProteomeXchange Consortium (http://proteomecentral.proteomexchange.org) via the PRIDE partner repository (PMID: 30395289) with the dataset identifier PXDXXXXXX. fPAR-CLIP sequencing data and RNAseq data are available on the NCBI Short-Read Archive (SRA) under the accession number GEO:XXXXX

SUPPLEMENTARY DATA

Supplementary Data are available at NAR online.

AUTHOR CONTRIBUTIONS

Vivian Lobo: Formal analysis, Methodology, Writing—review & editing. Iwona Nowak: Formal analysis, Methodology, Writing—original draft. Carola Fernandez: Formal analysis, Methodology, Writing—review & editing. Ana Iris Correa Muler: Methodology, Writing—review & editing. Jakub O. Westholm: Formal analysis, Methodology, Writing—review & editing. Hsiang-Chi Huang: Methodology, Writing—review & editing. Ivo Fabrik: Formal analysis, Writing—review & editing. Hang Thuy Huynh: Methodology, Writing—review & editing. Melis Kanik: Methodology, Writing—review & editing. Anetta Härtlova: Formal analysis, Writing—review & editing. Daniel Benhalevy: Formal analysis, Writing—review & editing. Davide Angeletti: Formal analysis, Methodology, Writing—review & editing. Aishe A. Sarshad: Conceptualization, Funding aquisition, Supervision, Formal analysis, Methodology, Writing—original draft.

ACKNOWLEDGEMENTS

The authors would like to acknowledge Dr. Ruth Palmer and Dr. Bengt Hallberg (University of Gothenburg) for the STE01 and CUT01 cancer cell lines, Maria Falkenberg (University of Gothenburg) for HAP1 cells. Volkan Sayin (University of Gothenburg) for providing us with Menadione. Dimitrios Anastaskis (NIIAMS, NIH) for technical support. Reyhaneh Rezaei for

technical support. Sequencing was performed by the SNP&SEQ Technology Platform in Uppsala. The facility is part of the National Genomics Infrastructure (NGI) Sweden and Science for Life Laboratory. The SNP&SEQ Platform is also supported by the Swedish Research Council and the Knut and Alice Wallenberg Foundation. We acknowleedge the Center for Cellular Imaging at the University of Gothenburg and the National Microscopy Infrastructure, NMI (VR-RFI 2019-00217) for providing assistance in microscopy.The proteomic analysis was performed at the Proteomics Core Facility at the University of Gothenburg, Sweden. The computations were enabled by resources in projects SNIC 2022/23-474 and SNIC 2022/22-996 provided by the National Academic Infrastructure for Supercomputing in Sweden (NAISS) at UPPMAX, funded by the Swedish Research Council through grant agreement no. 2022-06725.

FUNDING

Work in the Sarshad lab is supported by funding from Knut and Alice Wallenberg Foundation [grant number PAR 2020/228]; the Swedish research council [grant number 2019-01855]; the Swedish Society for Medical Research [grant number S19-0019]; Carl Trygger Foundation [grant number CTS 19:5]; the Swedish Medical Society [grant number SLS-934036]; Emil och Vera Cornell Foundation; Ake Wiberg Foundation [grant number M18-0091, M19-0243 and M20-0042]; Magnus Bergvall Foundation [grant number 2018-02791, 2019-03007 and 2020-03627]; Assar Gabrielssons Foundation [grant number FB18-109 and FB19-20]; Jeansson Foundation [grant number JS2019-0015]; Guvnor and Josef Anérs Foundation [grant number FB19-0063]; Ollie and Elof Ericsson Foundation and Olle Engkvist Byggmästare Foundation [grant number 193-614]. J.O.W is financially supported by the Knut and Alice Wallenberg Foundation as part of the National Bioinformatics Infrastructure Sweden at SciLifeLab. AH is supported by funding from Knut and Alice Wallenberg Foundation. DB is supported by funding from TAU Vice President for Research and Development Fund.

CONFLICT OF INTEREST

The authors declare no conflict of interest

REFERENCES

1. Hetzer MW. The nuclear envelope. Cold Spring Harb Perspect Biol. 2010;2(3):a000539.
2. Herrmann H, Aebi U. Intermediate Filaments: Structure and Assembly. Cold Spring Harb Perspect Biol. 2016;8(11):a018242.
3. Butin-Israeli V, Adam SA, Goldman AE, Goldman RD. Nuclear lamin functions and disease. Trends Genet. 2012;28(9):464-471.
4. Alcorta-Sevillano N, Macías I, Infante A, Rodríguez CI. Deciphering the Relevance of Bone ECM Signaling. Cells. 2020;9(12):2630.
5. Bouzid T, Kim E, Riehl BD, et al. The LINC complex, mechanotransduction, and mesenchymal stem cell function and fate. J Biol Eng. 2019;13:68.
6. Guerreiro I, Kind J. Spatial chromatin organization and gene regulation at the nuclear lamina. Curr Opin Genet Dev. 2019;55:19-25.
7. Melcer S, Hezroni H, Rand E, et al. Histone modifications and lamin A regulate chromatin protein dynamics in early embryonic stem cell differentiation. Nat Commun. 2012;3:910.
8. Bitman-Lotan E, Orian A. Nuclear organization and regulation of the differentiated state. Cell Mol Life Sci. 2021;78(7):3141-3158.
9. Dubik N, Mai S. Lamin A/C: Function in Normal and Tumor Cells. Cancers (Basel). 2020;12(12):3688.
10. Lee YS, Dutta A. MicroRNAs in cancer. Annu Rev Pathol. 2009;4:199-227.
11. Bartel DP. Metazoan MicroRNAs. Cell. 2018;173(1):20-51.
12. Peters L, Meister G. Argonaute proteins: mediators of RNA silencing. Mol Cell. 2007;26(5):611-623.
13. Kelly TJ, Suzuki HI, Zamudio JR, Suzuki M, Sharp PA. Sequestration of microRNA-mediated target repression by the Ago2-associated RNA-binding protein FAM120A. RNA. 2019;25(10):1291-1297.
14. Wilczynska A, Bushell M. The complexity of miRNA-mediated repression. Cell Death Differ. 2015;22(1):22-33.
15. Zeng Y, Cullen BR. RNA interference in human cells is restricted to the cytoplasm. RNA. 2002;8(7):855-860.

16. Vickers TA, Koo S, Bennett CF, Crooke ST, Dean NM, Baker BF. Efficient reduction of target RNAs by small interfering RNA and RNase H-dependent antisense agents. A comparative analysis. J Biol Chem. 2003;278(9):7108-7118.
17. Weinmann L, Höck J, Ivacevic T, et al. Importin 8 is a gene silencing factor that targets argonaute proteins to distinct mRNAs. Cell. 2009;136(3):496-507.
18. Johnson KC, Corey DR. RNAi in cell nuclei: potential for a new layer of biological regulation and a new strategy for therapeutic discovery. RNA. 2023;29(4):415-422.
19. Nazer E, Gómez Acuña L, Kornblihtt AR. Seeking the truth behind the myth: Argonaute tales from "nuclearland". Mol Cell. 2022;82(3):503-513.
20. Sarshad AA, Juan AH, Muler AIC, et al. Argonaute-miRNA Complexes Silence Target mRNAs in the Nucleus of Mammalian Stem Cells. Mol Cell. 2018;71(6):1040-1050.e8.
21. Nowak I, Sarshad AA. Argonaute Proteins Take Center Stage in Cancers. Cancers (Basel). 2021;13(4):788.
22. Chu Y, Yokota S, Liu J, Kilikevicius A, Johnson KC, Corey DR. Argonaute binding within human nuclear RNA and its impact on alternative splicing. RNA. 2021;27(9):991-1003.
23. Shen J, Xia W, Khotskaya YB, et al. EGFR modulates microRNA maturation in response to hypoxia through phosphorylation of AGO2. Nature. 2013;497(7449):383-387.
24. Liu T, Zhang H, Fang J, et al. AGO2 phosphorylation by c-Src kinase promotes tumorigenesis. Neoplasia. 2020;22(3):129-141.
25. Horman SR, Janas MM, Litterst C, et al. Akt-mediated phosphorylation of argonaute 2 downregulates cleavage and upregulates translational repression of MicroRNA targets. Mol Cell. 2013;50(3):356-367.
26. Sala L, Chandrasekhar S, Cosby RL, La Rocca G, Macfarlan TS, Awasthi P, Chari R, Kruhlak M, Vidigal JA. AGO2 silences mobile transposons in the nucleus of quiescent cells. biorXiv https://doi.org/10.1101/2022.07.17.500356, Posted July 17, 2022., pre-print: not peer-reviewed.
27. Welte T, Goulois A, Stadler MB, Hess D, Soneson C, Neagu A, Azzi C, Lübke MJ, Seebacher J, Schmidt I, Estoppey D, Nigsch F, Reece-Hoyes J, Hoepfner D, Großhans H. Convergence of multiple RNA-silencing pathways on GW182/TNRC6. bioRxiv preprint doi: https://doi.org/10.1101/2023.04.20.537632; this version posted April 20, 2023.
28. Sallis S, Bérubé-Simard FA, Grondin B, et al. The CHARGE syndrome-associated protein FAM172A controls AGO2 nuclear import. Life Sci Alliance. 2023;6(8):e202302133.

29. Wei Y, Li L, Wang D, Zhang CY, Zen K. Importin 8 regulates the transport of mature microRNAs into the cell nucleus. J Biol Chem. 2014;289(15):10270-10275.
30. Griffin KN, Walters BW, Li H, Wang H, Biancon G, Tebaldi T, Kaya CB, Kanyo J, Lam TT, Cox AL, Halene S, Chung JJ, Lesch BJ. Widespread association of the Argonaute protein AGO2 with meiotic chromatin suggests a distinct nuclear function in mammalian male reproduction. Genome Res. 2022;32(9):1655-1668.
31. Ohrt T, Mütze J, Staroske W, Weinmann L, Höck J, Crell K, Meister G, Schwille P. Fluorescence correlation spectroscopy and fluorescence cross-correlation spectroscopy reveal the cytoplasmic origination of loaded nuclear RISC in vivo in human cells. Nucleic Acids Res. 2008;36(20):6439-6449.
32. Gagnon KT, Li L, Janowski BA, Corey DR. Analysis of nuclear RNA interference in human cells by subcellular fractionation and Argonaute loading. Nat Protoc. 2014;9(9):2045-2060.
33. Sakuma T, Nakade S, Sakane Y, Suzuki KT, Yamamoto T. MMEJ-assisted gene knock-in using TALENs and CRISPR-Cas9 with the PITCh systems. Nat Protoc. 2016;11(1):118-133.
34. Tandon N, Thakkar KN, LaGory EL, Liu Y, Giaccia AJ. Generation of Stable Expression Mammalian Cell Lines Using Lentivirus. Bio Protoc. 2018;8(21):e3073.
35. Benhalevy D, Hafner M. Proximity-CLIP Provides a Snapshot of Protein-Occupied RNA Elements at Subcellular Resolution and Transcriptome-Wide Scale. Methods Mol Biol.
36. Hauptmann J, Schraivogel D, Bruckmann A, Manickavel S, Jakob L, Eichner N, Pfaff J, Urban M, Sprunck S, Hafner M, Tuschl T, Deutzmann R, Meister G. Biochemical isolation of Argonaute protein complexes by Ago-APP. Proc Natl Acad Sci U S A. 2015;112(38):11841-11845.
37. Wiśniewski JR, Zougman A, Nagaraj N, Mann M. Universal sample preparation method for proteome analysis. Nat Methods. 2009;6(5):359-362.
38. Ewels PA, Peltzer A, Fillinger S, Patel H, Alneberg J, Wilm A, Garcia MU, Di Tommaso P, Nahnsen S. The nf-core framework for community-curated bioinformatics pipelines. Nat Biotechnol. 2020;38(3):276-278.
39. Love MI, Huber W, Anders S. Moderated estimation of fold change and dispersion for RNA-seq data with DESeq2. Genome Biol. 2014;15(12):550.
40. Wang L, Wang S, Li W. RSeQC: quality control of RNA-seq experiments. Bioinformatics. 2012 Aug 15;28(16):2184-5.

41. Anastasakis DG, Jacob A, Konstantinidou P, Meguro K, Claypool D, Cekan P, Haase AD, Hafner M. A non-radioactive, improved PAR-CLIP and small RNA cDNA library preparation protocol. Nucleic Acids Res. 2021;49(8):e45.
42. Martin M Cutadapt removes adapter sequences from high-throughput sequencing reads. EMBnet.journal. [Online] 2011:17:1.
43. Corcoran DL, Georgiev S, Mukherjee N, Gottwein E, Skalsky RL, Keene JD, Ohler U. PARalyzer: definition of RNA binding sites from PAR-CLIP short-read sequence data. Genome Biol. 2011;12(8):R79.
44. Li, X., Pritykin, Y., Concepcion, C. P., Lu, Y., La Rocca, G., Zhang, M., King, B., Cook, P. J., Au, Y. W., Popow, O., Paulo, J. A., Otis, H. G., Mastroleo, C., Ogrodowski, P., Schreiner, R., Haigis, K. M., Betel, D., Leslie, C. S., & Ventura, A. High-Resolution In Vivo Identification of miRNA Targets by Halo-Enhanced Ago2 Pull-Down. Molecular cell, 79(1), 2020;167–179.e11.
45. Rentschler M, Chen Y, Pahl J, Soria-Martinez L, Braumüller H, Brenner E, Bischof O, Röcken M, Wieder T. Nuclear Translocation of Argonaute 2 in Cytokine-Induced Senescence. Cell Physiol Biochem. 2018;51(3):1103-1118.
46. Chu Y, Yue X, Younger ST, Janowski BA, Corey DR. Involvement of argonaute proteins in gene silencing and activation by RNAs complementary to a non-coding transcript at the progesterone receptor promoter. Nucleic Acids Res. 2010;38(21):7736-48.
47. Tan GS, Garchow BG, Liu X, Yeung J, Morris JP 4th, Cuellar TL, McManus MT, Kiriakidou M. Expanded RNA-binding activities of mammalian Argonaute 2. Nucleic Acids Res. 200937(22):7533-45.
48. Cautain B, Hill R, de Pedro N, Link W. Components and regulation of nuclear transport processes. FEBS J. 2015;282(3):445-62.
49. Wang KP, Bai Y, Wang J, Zhang JZ. Morphine protects SH-SY5Y human neuroblastoma cells against Dickkopf1-induced apoptosis. Mol Med Rep. 2015 ;11(2):1174-80.
50. Lelliott EJ, Cullinane C, Martin CA, Walker R, Ramsbottom KM, Souza-Fonseca-Guimaraes F, Abuhammad S, Michie J, Kirby L, Young RJ, Slater A, Lau P, Meeth K, Oliaro J, Haynes N, McArthur GA, Sheppard KE. A novel immunogenic mouse model of melanoma for the preclinical assessment of combination targeted and immune-based therapy. Sci Rep. 2019;9(1):1225.
51. Luo YB, Mastaglia FL, Wilton SD. Normal and aberrant splicing of LMNA. J Med Genet. 2014;51(4):215-23.

52. Subramanian A, Tamayo P, Mootha VK, Mukherjee S, Ebert BL, Gillette MA, Paulovich A, Pomeroy SL, Golub TR, Lander ES, Mesirov JP. Gene set enrichment analysis: a knowledge-based approach for interpreting genome-wide expression profiles. Proc Natl Acad Sci U S A. 2005;102(43):15545-50.
53. Mootha VK, Lindgren CM, Eriksson KF, Subramanian A, Sihag S, Lehar J, Puigserver P, Carlsson E, Ridderstråle M, Laurila E, Houstis N, Daly MJ, Patterson N, Mesirov JP, Golub TR, Tamayo P, Spiegelman B, Lander ES, Hirschhorn JN, Altshuler D, Groop LC. PGC-1alpha-responsive genes involved in oxidative phosphorylation are coordinately downregulated in human diabetes. Nat Genet. 2003;34(3):267-73.
54. Wang S, Sun X, Yi C, Zhang D, Lin X, Sun X, Chen H, Jin M. AGO2 Negatively Regulates Type I Interferon Signaling Pathway by Competition Binding IRF3 with CBP/p300. Front Cell Infect Microbiol. 2017;7:195.
55. Tanaka M, Sasaki K, Kamata R, Hoshino Y, Yanagihara K, Sakai R. A novel RNA-binding protein, Ossa/C9orf10, regulates activity of Src kinases to protect cells from oxidative stress-induced apoptosis. Mol Cell Biol. 2009;29(2):402-13.
56. Kalantari R, Hicks JA, Li L, Gagnon KT, Sridhara V, Lemoff A, Mirzaei H, Corey DR. Stable association of RNAi machinery is conserved between the cytoplasm and nucleus of human cells. RNA. 2016;22(7):1085-98.
57. Qin W, Cho KF, Cavanagh PE, Ting AY. Deciphering molecular interactions by proximity labeling. Nat Methods. 2021;18(2):133-143.
58. Bell ES, Shah P, Zuela-Sopilniak N, Kim D, Varlet AA, Morival JLP, McGregor AL, Isermann P, Davidson PM, Elacqua JJ, Lakins JN, Vahdat L, Weaver VM, Smolka MB, Span PN, Lammerding J. Low lamin A levels enhance confined cell migration and metastatic capacity in breast cancer. Oncogene. 2022;41(36):4211-4230.
59. Roskoski R Jr. Src protein-tyrosine kinase structure, mechanism, and small molecule inhibitors. Pharmacol Res. 2015;94:9-25.
60. Wecker H, Waller CF. Afatinib. Recent Results Cancer Res. 2018;211:199-215.
61. Romero-Cordoba SL, Salido-Guadarrama I, Rodriguez-Dorantes M, Hidalgo-Miranda A. miRNA biogenesis: biological impact in the development of cancer. Cancer Biol Ther. 2014;15(11):1444-55.
62. Stalder L, Heusermann W, Sokol L, Trojer D, Wirz J, Hean J, Fritzsche A, Aeschimann F, Pfanzagl V, Basselet P, Weiler J, Hintersteiner M, Morrissey DV, Meisner-Kober NC. The

rough endoplasmatic reticulum is a central nucleation site of siRNA-mediated RNA silencing. EMBO J. 2013;32(8):1115-27.

63. Sen GL, Blau HM. Argonaute 2/RISC resides in sites of mammalian mRNA decay known as cytoplasmic bodies. Nat Cell Biol. 2005;7(6):633-6.
64. Hirsch M, Helm M. Live cell imaging of duplex siRNA intracellular trafficking. Nucleic Acids Res. 2015;43(9):4650-60.
65. Goldberg MW. Nuclear pore complex tethers to the cytoskeleton. Semin Cell Dev Biol. 2017;68:52-58.
66. Denais C, Lammerding J. Nuclear mechanics in cancer. Adv Exp Med Biol. 2014;773:435-70.
67. Irianto J, Pfeifer CR, Ivanovska IL, Swift J, Discher DE. Nuclear lamins in cancer. Cell Mol Bioeng. 2016;9(2):258-267.
68. Eckersley-Maslin MA, Bergmann JH, Lazar Z, Spector DL. Lamin A/C is expressed in pluripotent mouse embryonic stem cells. Nucleus. 2013;4(1):53-60.
69. Heo SJ, Cosgrove BD, Dai EN, Mauck RL. Mechano-adaptation of the stem cell nucleus. Nucleus. 2018 ;9(1):9-19.
70. Kim BS, Jung JS, Jang JH, Kang KS, Kang SK. Nuclear Argonaute 2 regulates adipose tissue-derived stem cell survival through direct control of miR10b and selenoprotein N1 expression. Aging Cell. 2011;10(2):277-91.
71. Katz S, Cussigh D, Urbán N, Blomfield I, Guillemot F, Bally-Cuif L, Coolen M. A Nuclear Role for miR-9 and Argonaute Proteins in Balancing Quiescent and Activated Neural Stem Cell States. Cell Rep. 2016;17(5):1383-1398.
72. Adams BD, Claffey KP, White BA. Argonaute-2 expression is regulated by epidermal growth factor receptor and mitogen-activated protein kinase signaling and correlates with a transformed phenotype in breast cancer cells. Endocrinology. 2009;150(1):14-23.
73. Yang M, Haase AD, Huang FK, Coulis G, Rivera KD, Dickinson BC, Chang CJ, Pappin DJ, Neubert TA, Hannon GJ, Boivin B, Tonks NK. Dephosphorylation of tyrosine 393 in argonaute 2 by protein tyrosine phosphatase 1B regulates gene silencing in oncogenic RAS-induced senescence. Mol Cell. 2014;55(5):782-90.
74. Järås M, Miller PG, Chu LP, Puram RV, Fink EC, Schneider RK, Al-Shahrour F, Peña P, Breyfogle LJ, Hartwell KA, McConkey ME, Cowley GS, Root DE, Kharas MG, Mullally A, Ebert

BL. Csnk1a1 inhibition has p53-dependent therapeutic efficacy in acute myeloid leukemia. J Exp Med. 2014;211(4):605-12.

75. Castanotto D, Zhang X, Alluin J, Zhang X, Rüger J, Armstrong B, Rossi J, Riggs A, Stein CA. A stress-induced response complex (SIRC) shuttles miRNAs, siRNAs, and oligonucleotides to the nucleus. Proc Natl Acad Sci U S A. 2018;115(25):E5756-E5765.
76. Riggs CL, Kedersha N, Ivanov P, Anderson P. Mammalian stress granules and P bodies at a glance. J Cell Sci. 2020;133(16):jcs242487.

TABLE AND FIGURES LEGENDS

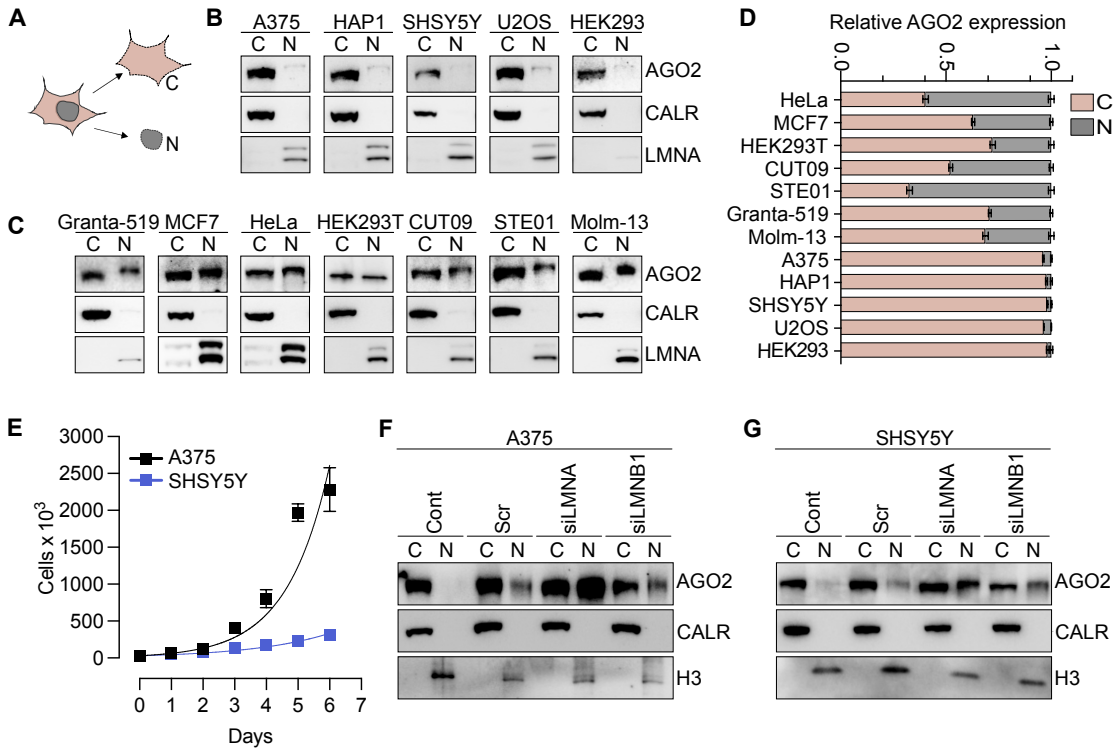

Figure 1. Low *LMNA* expression triggers AGO2 nuclear translocation. (A) Schematic representation of biochemical fractionation of cytoplasmic and nuclear fractions. Representative images of AGO2 immunoblots from cytoplasmic and nuclear fractions in a panel of **(B)** nuclear AGO2 negative and **(C)** nuclear AGO2 positive human cell lines. **(D)** Relative ratio of nuclear and cytoplasmic AGO2 fractions in the studied cell lines. **(E)** Cell proliferation assay for A375 and SHSY5Y cells. Exponential (Malthusian) growth for proliferation assays line was fitted for the data sets. Representative images of AGO2 immunoblots from cytoplasmic and nuclear fractions in cells transfected with the siRNAs for LMNA and LMNB1 in **(F)** A375 and **(G)** SHSY5Y cells. For biochemical fractionation experiments CALR served as cytoplasmic marker while LMNA and H3 as nuclear markers. C, cytoplasmic fraction; N, nuclear fraction; CALR, Calreticulin; LMNA, Lamin A/C; H3, Histone H3; Cont, cells treated with Lipofectamine RNAiMAX transfection agent; Scr, cells transfected with scrambled oligonucleotide; si*LMNA*, cells transfected with siRNAs against *LMNA*; si*LMNB1*, cells transfected with siRNAs against *LMNB1*. Graphs presented in the figure represent results calculated from three independent experiments, and presented as the mean ± standard deviation.

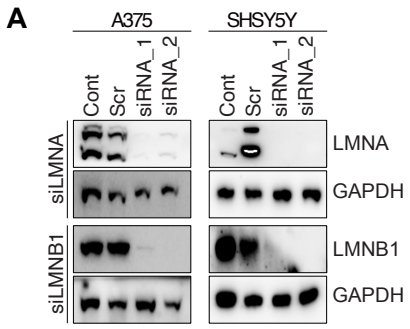

Supplemental Figure 1 related to main Figure 1 (A) Representative images of Lamin A/C and Lamin B1 immunoblots in A375 and SHSY5Y cells transfected with siRNAs against LMNA and LMNB, respectively. GAPDH was used as a loading control. LMNA, Lamin A/C; LMNB1, Lamin B1; Cont, cells treated with Lipofectamine RNAiMAX transfection agent; siLMNA, cells transfected with siRNAs against LMNA; siLMNB1, cells transfected with siRNAs against LMNB1.

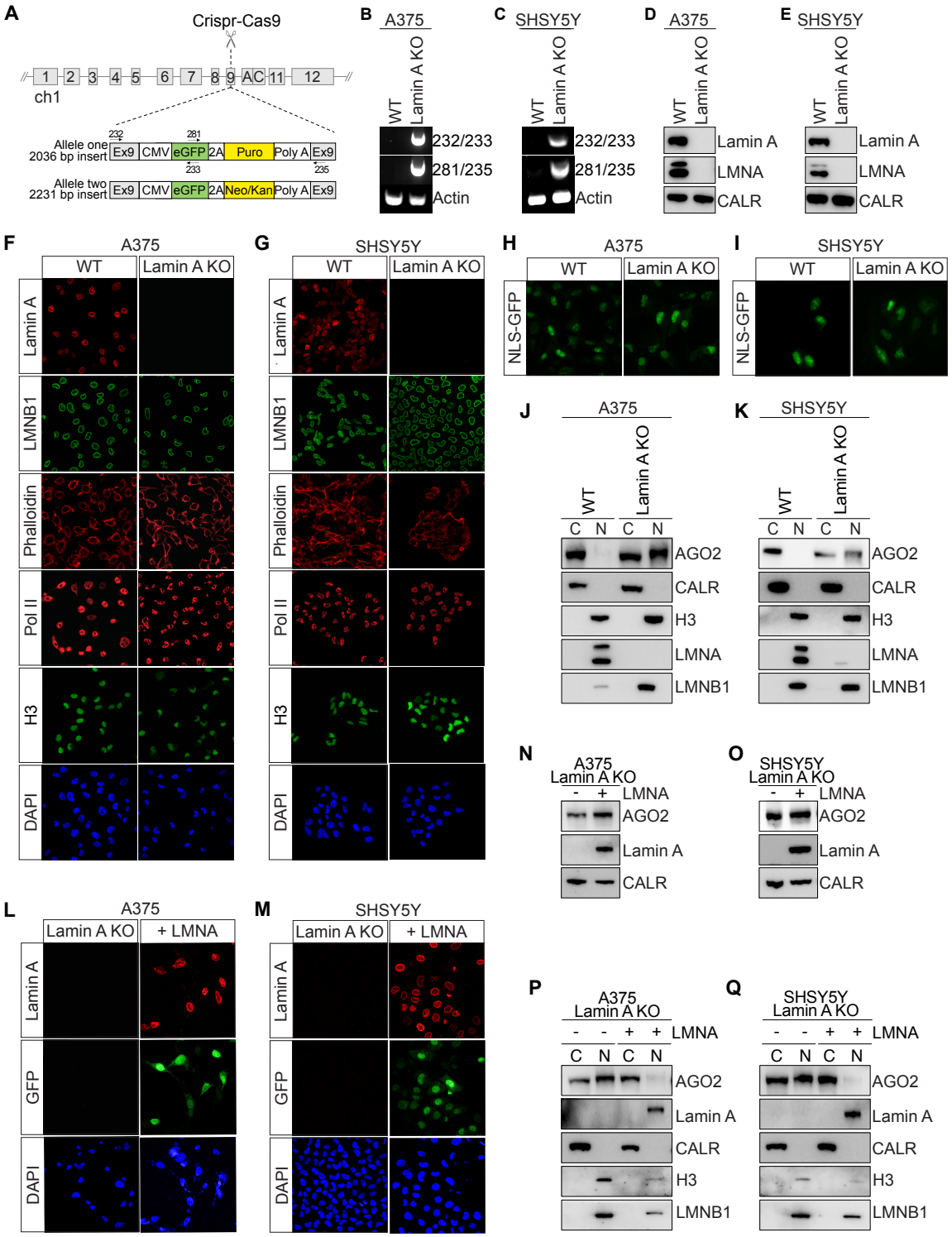

Figure 2. Lamin A KO causes significant nuclear translocation of AGO2 protein. (A) Graphical representation of the CRISPR-Cas9 strategy used in the study. Numbers and arrows illustrate the location and direction of primers used in PCR experiments. PCR amplification of Actin and antibiotic resistance/eGFP cassette in **(B)** A375 and **(C)** SHSY5Y Lamin A KO cells. Primer numbers are indicated. Representative images of Lamin A, Lamin A/C and Calreticulin immunoblots from **(D)** A375 and **(E)** SHSY5Y WT and Lamin A KO cells. Immunofluorescence staining of Lamin A, LMNB1, Phalloidin, Pol II, H3 and DAPI in **(F)** A375 and **(G)** SHSY5Y WT

and Lamin A KO cells. Representative images of NLS-GFP fluorescent signal in **(H)** A375 and **(I)** SHSY5Y WT and Lamin A KO cells. Representative images of AGO2 immunoblots from cytoplasmic and nuclear fractions in **(J)** A375 and **(K)** SHSY5Y WT and Lamin A KO cells. Immunofluorescence staining of Lamin A, GFP, and DAPI in **(L)** A375 and **(M)** SHSY5Y Lamin A KO cells and Lamin A KO Lamin A/C overexpressing cells. Representative images of AGO2 and Lamin A immunoblots from **(N)** A375 and **(O)** SHSY5Y Lamin A KO and Lamin A KO Lamin A/C overexpressing cells. CALR was used as a loading control. Representative images of AGO2 and Lamin A immunoblots from cytoplasmic and nuclear fractions in Lamin A KO and Lamin A KO Lamin A/C overexpressing **(P)** A375 and **(Q)** SHSY5Y cells. For biochemical fractionation experiments the endoplasmic reticulum protein Calreticulin served as cytoplasmic marker while H3 and LMNB1 served as nuclear markers. WT, wild-type cells; Lamin A KO, Lamin A knock out cells; LMNA, Lamin A/C; CALR, Calreticulin; Pol II, RNA polymerase II; H3, Histone H3; LMNB1, Lamin B1.

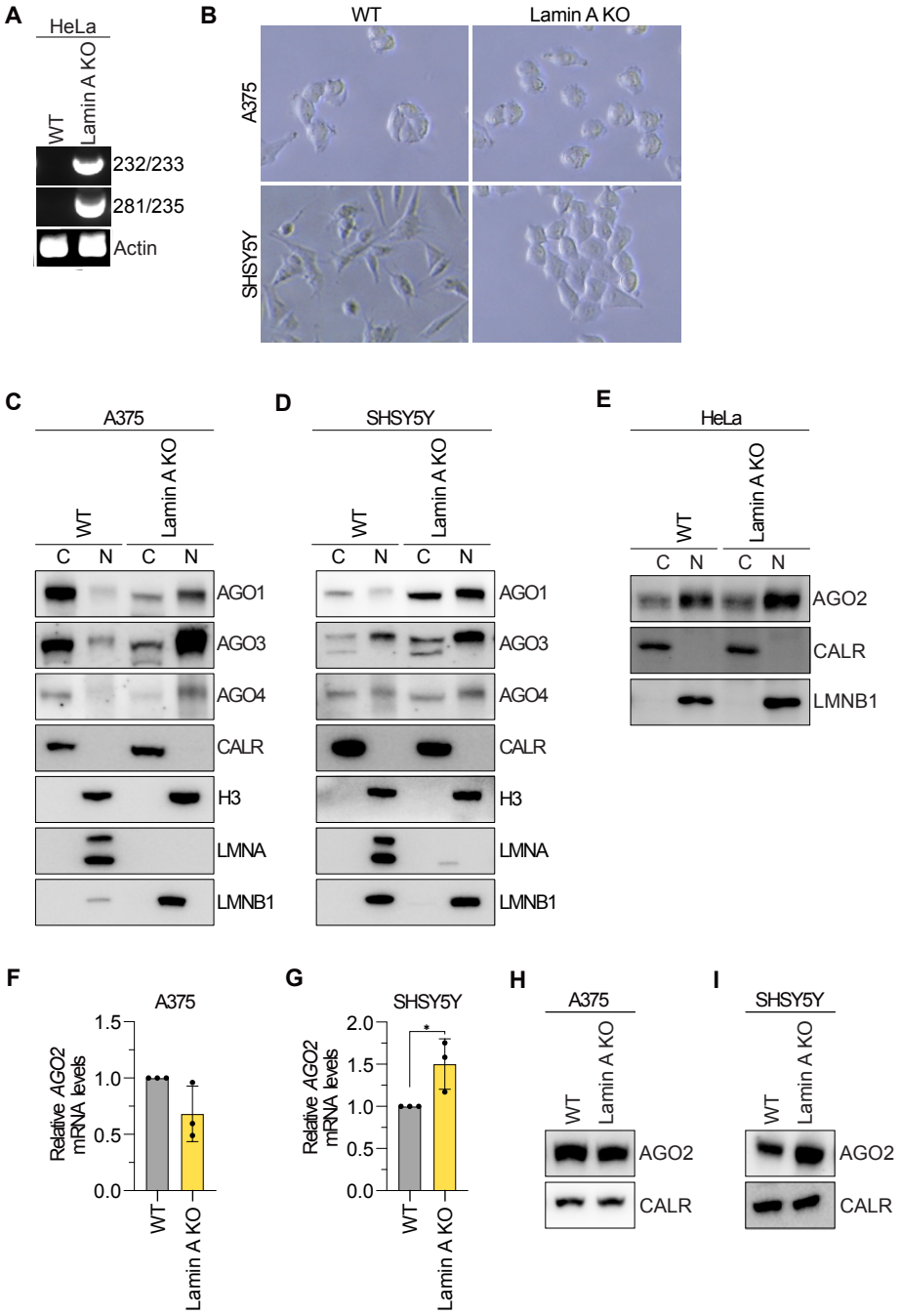

Supplemental Figure 2 related to main Figure 2. **(A)** PCR amplification of actin and antibiotic resistance/eGFP cassette in HeLa Lamin A KO cells. Primer numbers are indicated. **(B)** Bright field microscopy pictures of A375 and SHSY5Y WT and Lamin A KO cells. Representative images of AGO1,3 and 4 immunoblots from cytoplasmic and nuclear fractions in **(C)** A375 and **(D)** SHSY5Y WT and Lamin A KO cells. **(E)** Representative images of AGO1,3, immunoblots from cytoplasmic and nuclear fractions in HeLa WT and Lamin A KO cells. For biochemical fractionation experiments CALR served as cytoplasmic marker while LMNB1 and H3 served as nuclear markers. AGO2 mRNA levels in Lamin A KO vs WT **(F)** A375 and **(G)** SHSY5Y cells determined using RT-qPCR and 18S rRNA as a reference gene, values for WT cells set as 1. Results were calculated from three independent experiments, additionally performed

in three technical triplicates, and presented as the mean ± standard deviation. Representative images of AGO2 immunoblots from **(H)** A375 and **(I)** SHSY5Y WT and Lamin A KO cells. CALR was used as a loading control. WT, wild-type cells; Lamin A KO, Lamin A KO cells; C, cytoplasmic fraction; N, nuclear fraction; CALR, calreticulin; LMNB1, Lamin B1; H3, Histone H3. *P<0.05.

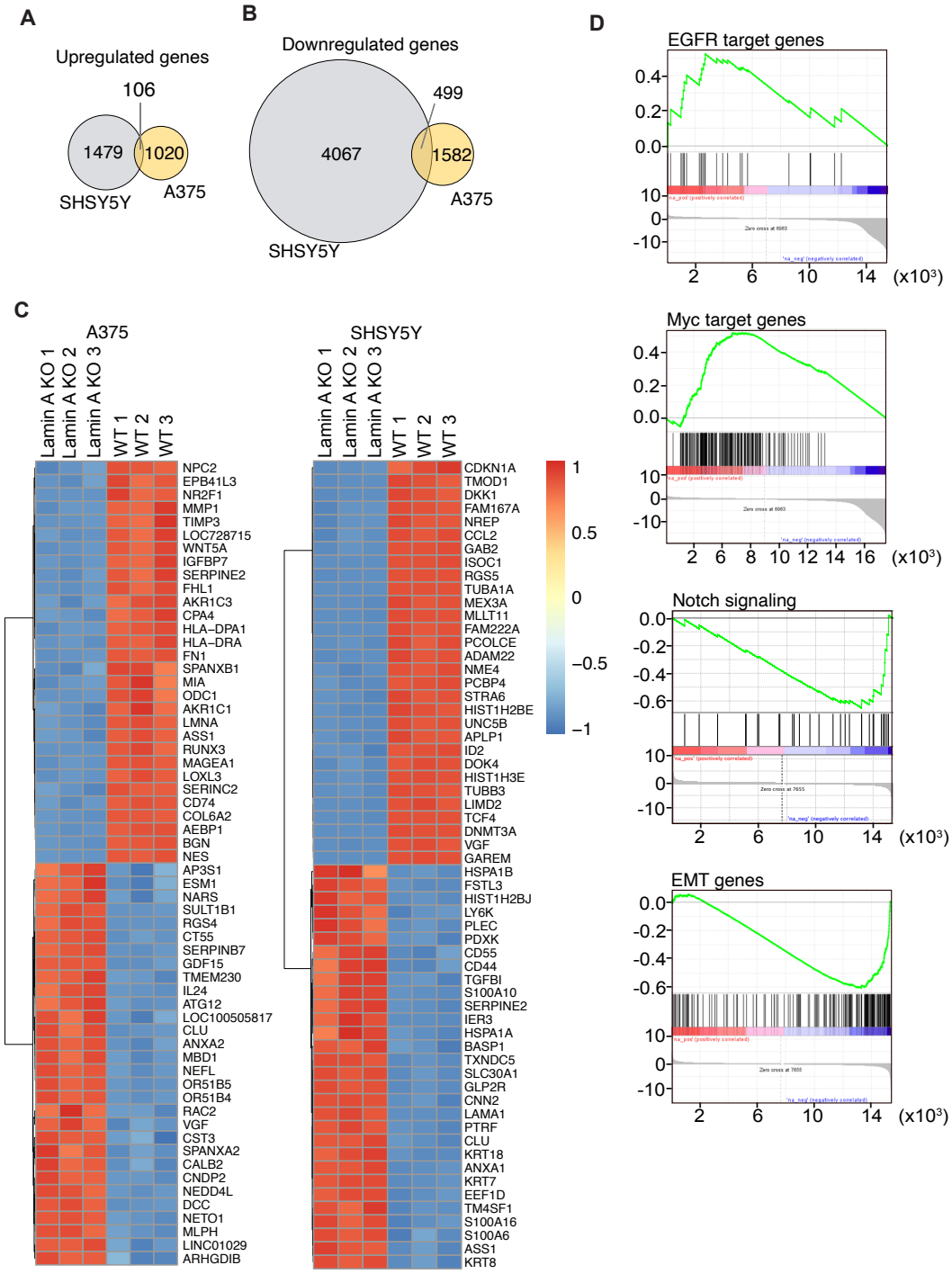

Figure 3. Lamin A KO triggers potent changes in gene expression in SHSY5Y and A375 cells. Venn diagram of the overlap of genes **(A)** upregulated and **(B)** downregulated in SHSY5Y and A375 cells upon Lamin A KO. **(C)** Heatmap of expression changes of the top 30 downregulated and upregulated genes in A375 and SHSY5Y Lamin A KO vs WT cells. **(D)** GSEA analysis of RNAseq data. WT, wild-type cells; Lamin A KO, Lamin A knock out cells; GSEA, Gene Set Enrichment Analysis.

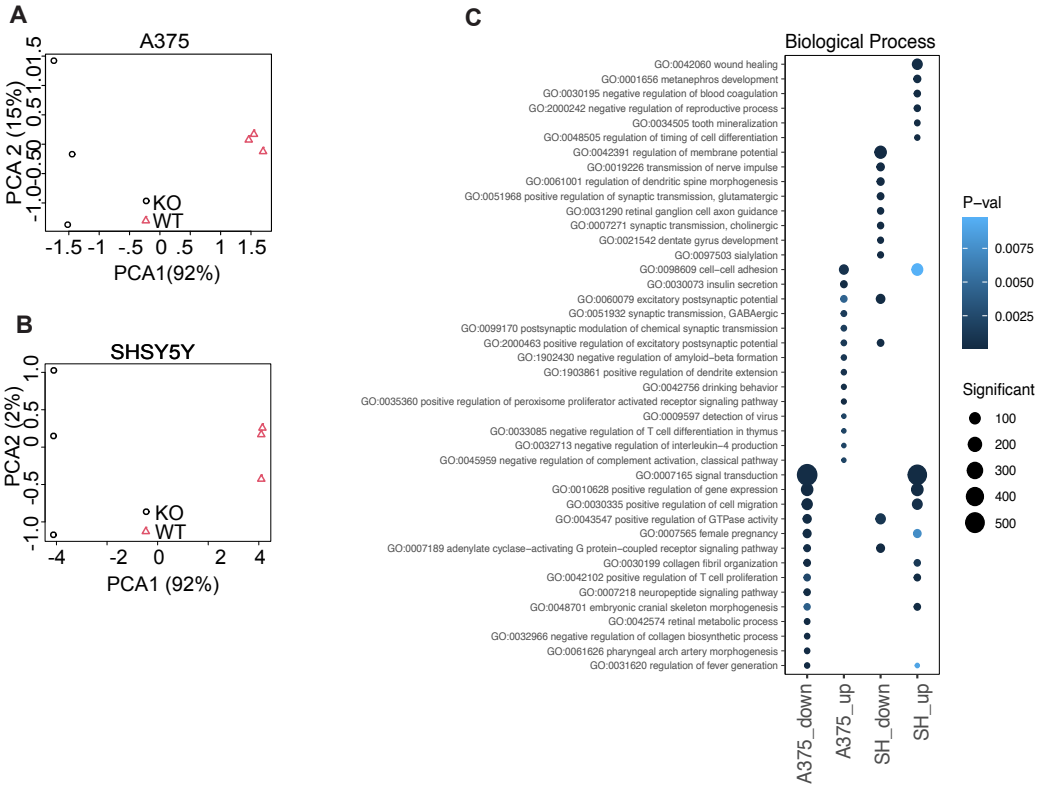

Supplemental Figure 3 related to main Figure 3. PCA of three independent RNAseq experiments in **(A)** A375 and **(B)** SHSY5Y. **(C)** Biological process annotations provided GO for transcripts that were significantly downregulated and upregulated upon Lamin A KO in A375 and SHSY5Y cells. PCA, principal component analysis; WT, wild-type cells; KO, Lamin A KO cells; GO, Gene Ontology; BP, biological processes.

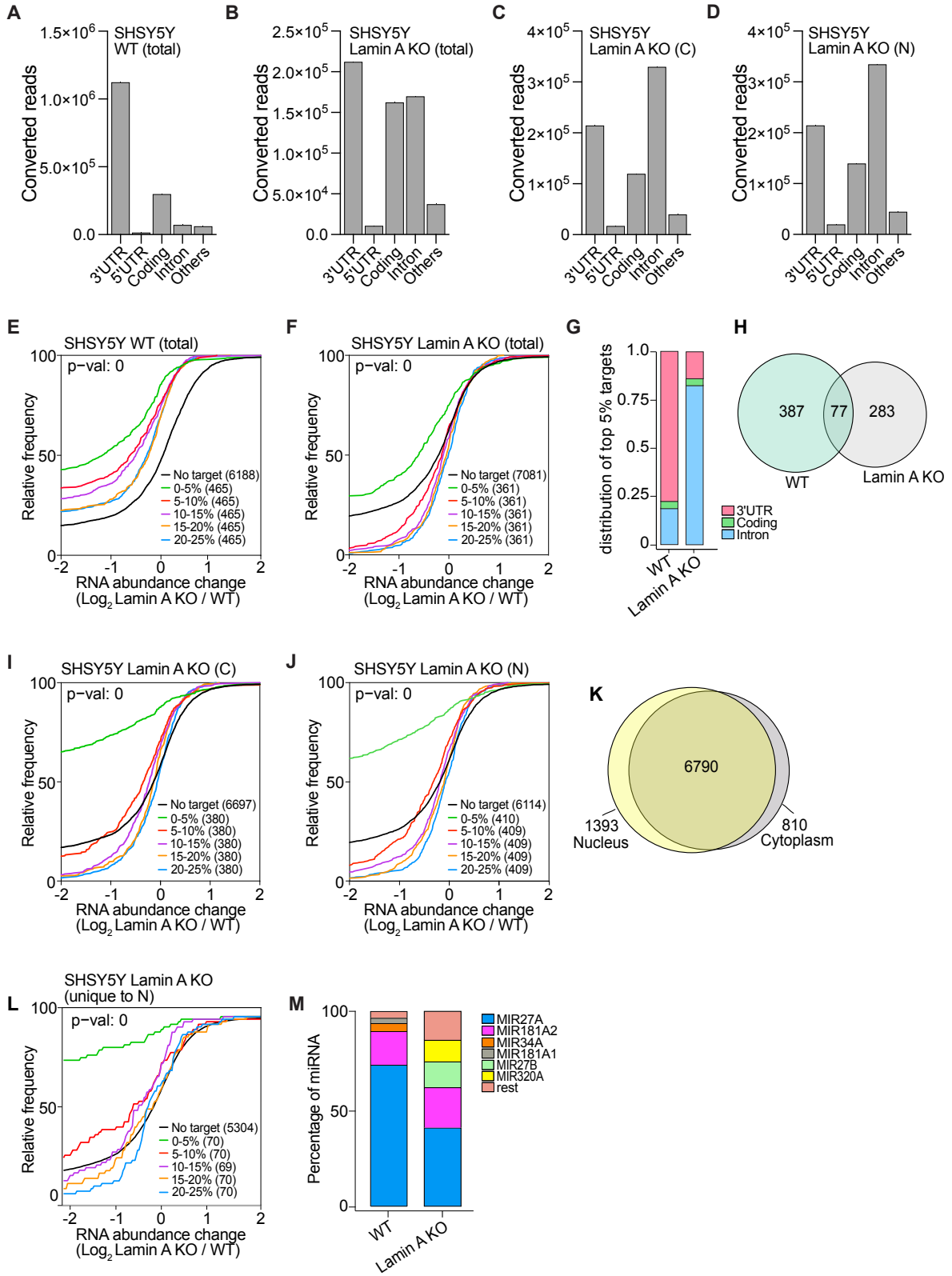

Figure 4. Nuclear RNAi is reduced upon Lamin A KO. Distribution of AGO fPAR-CLIP sequence reads across target RNAs in SHSY5Y **(A)** WT total lysate and **(B)** Lamin A KO total lysates **(C)** cytoplasmic and **(D)** nuclear fractions. Cumulative distribution of abundance changes in RNA in SHSY5Y **(E)** WT and **(F)** Lamin A KO cells. **(G)** Distribution of AGO fPAR-

CLIP sequence reads across the top 5% target RNAs in SHSY5Y WT and Lamin A KO total lysates. **(H)** Venn diagram of the overlap between the top 5% of AGO fPAR-CLIP targets in SHSY5Y WT and Lamin A KO cells. Cumulative distribution of abundance changes in RNA in SHSY5Y Lamin A KO **(I)** cytoplasmic and **(J)** nuclear lysates. **(K)** Venn diagram of the overlap between AGO fPAR-CLIP targets in SHSY5Y Lamin A KO cytoplasmic and nuclear lysate. **(L)** Cumulative distribution of abundance changes in RNA in SHSY5Y Lamin A KO exclusively nuclear AGO fPARCLIP targets. **(M)** Distribution of miRNA fPAR-CLIP targets in SHSY5Y WT and Lamin A KO total lysates. For cumulative distribution assays the targets were ranked by number of binding sites from top 5% to top 20-25% and compared to non-targets. WT, wild-type cells, Lamin A KO, Lamin A knock out cells; C, cytoplasmic fraction; N, nuclear fraction; fPAR-CLIP, fluorescent photoactivatable ribonucleoside-enhanced crosslinking and immunoprecipitation.

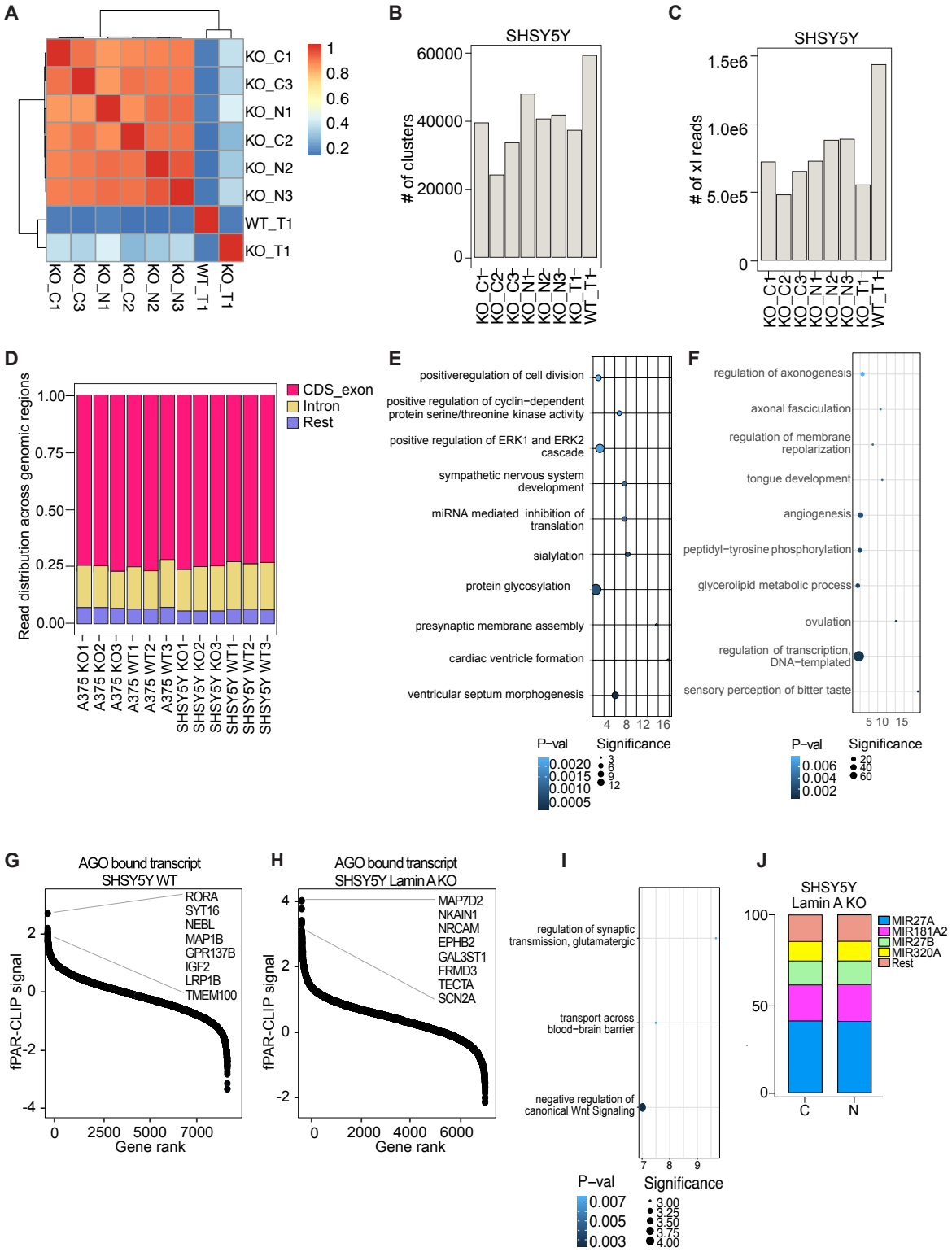

Supplemental Figure 4 related to main Figure 4. (A) Heatmap representing correlation between fPAR-CLIP libraries. **(B)** Overall cluster numbers for each AGO fPAR-CLIP experiments. **(C)** Number of crosslinked reads for respective fPAR-CLIP experiments. **(D)** Distribution of genomic regions annotated in RNAseq experiments. **(E)** GO analysis for exclusively AGO fPAR-CLIP targets found in WT, but not Lamin A KO total fPAR-CLIP libraries. **(F)** GO analysis for

exclusively AGO fPAR-CLIP targets found in Lamin A KO, but not in WT total fPAR-CLIP libraries. Top AGO fPAR-CLIP targets in SHSY5Y **(G)** WT and **(H)** Lamin A KO total lysates. **(I)** GO for exclusively nuclear AGO fPARCLIP targets in SHSY5Y Lamin A KO cells. **(J)** Distribution of miRNA fPAR-CLIP targets in SHSY5Y Lamin A KO cytoplasmic and nuclear lysates. WT, wild-type cells, Lamin A KO, Lamin A knock out cells; C, cytoplasmic fraction; N, nuclear fraction; fPAR-CLIP, fluorescent photoactivatable ribonucleoside-enhanced crosslinking and immunoprecipitation.

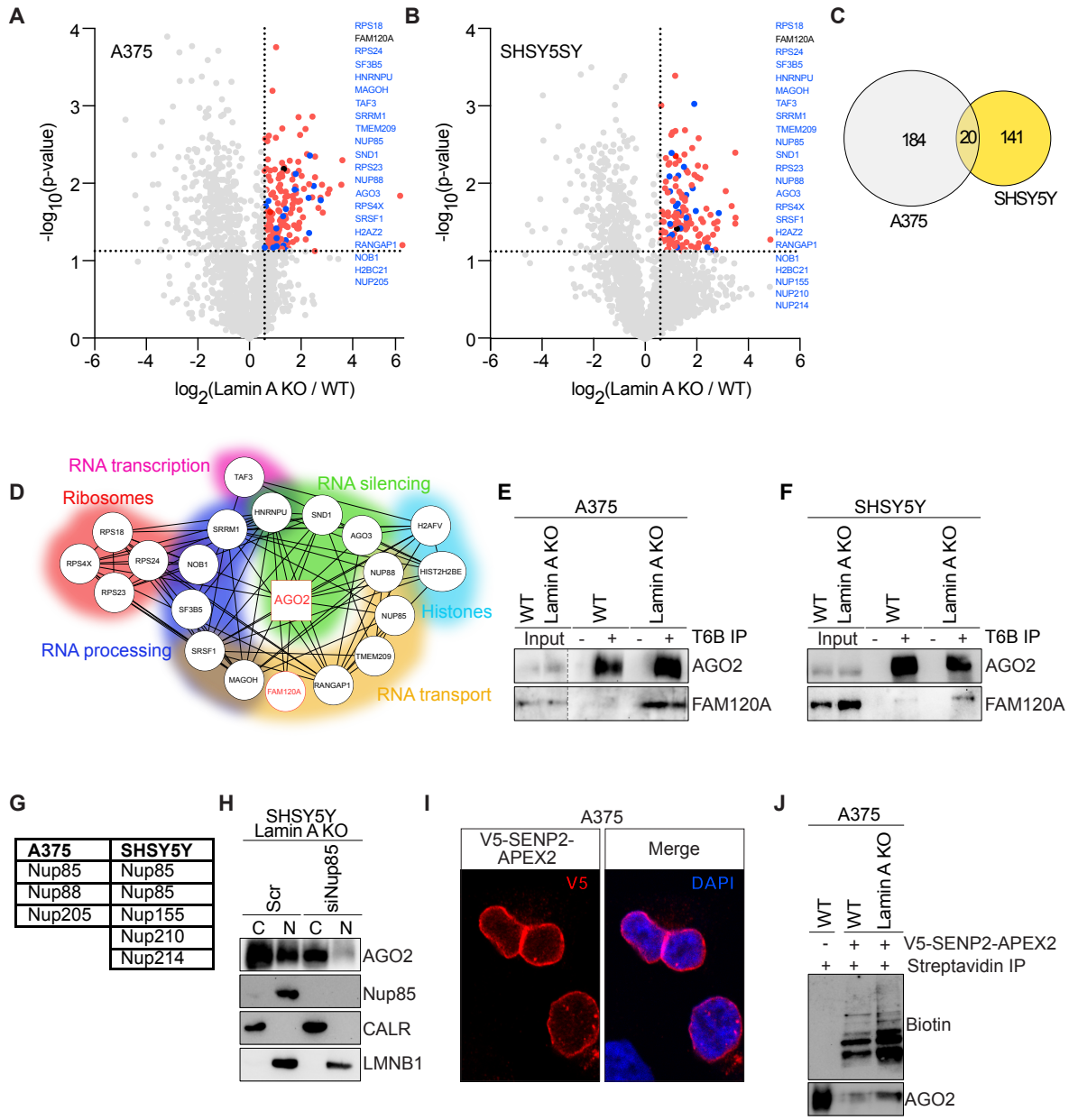

Figure 5. AGO2 interacts with proteins involved in RNA processing and transport in the nucleus of Lamin A KO cells. Volcano plots of mass spectrometry hits in Lamin A KO vs WT **(A)** A375 and **(B)** SHSY5Y nuclear lysates. Proteins significantly upregulated in Lamin A KO nucleus are indicated in red, blue and black. **C)** Venn diagram of significantly upregulated mass spec hits in the nucleus of Lamin A KO vs WT A375 (indicated in grey) and SHSY5Y (indicated in yellow) cells. **(D)** String analysis of significantly upregulated mass spec hits in the nucleus of Lamin A KO vs WT overlap between A375 and SHSY5Y cells. Representative images of AGO2 and FAM120A immunoblots from co-immunoprecipitation assay in **(E)** A375 and **(F)** SHSY5Y cells. **(G)** Nucleoporins significantly enriched in Lamin A KO vs WT nuclear AGO mass spectrometry. **(H)** Representative images of AGO2 and Nup85 immunoblots in cytoplasmic

and nuclear fractions of siRNAs transfected in SHSY5Y Lamin A KO cells. CALR served as cytoplasmic marker while LMNB1 served as nuclear marker. **(I)** Immunofluorescence staining of V5-SENP2-APEX2 in A375 WT SENP2-APEX2 and A375 Lamin A KO SENP2-APEX2 cells. **(J)** Representative image of biotin and AGO2 immunoblot of streptavidin affinity purification from A375 WT SENP2-APEX2 and A375 Lamin A KO SENP2-APEX2 cells as compared to parental cell line A375 WT. WT, wild-type cells; Lamin A KO, Lamin A knock out cells; C, cytoplasmic fraction; N, nuclear fraction; CALR, calreticulin; LMNB1, Lamin B1; Cont, cells treated with Lipofectamine RNAiMAX transfection agent; Scr, cells transfected with scrambled oligonucleotide; si*Nup85,* cells transfected with siRNAs against *Nup85;* V5-SENP2-APEX2, cells expressing V5-SENP2-APEX2 protein.

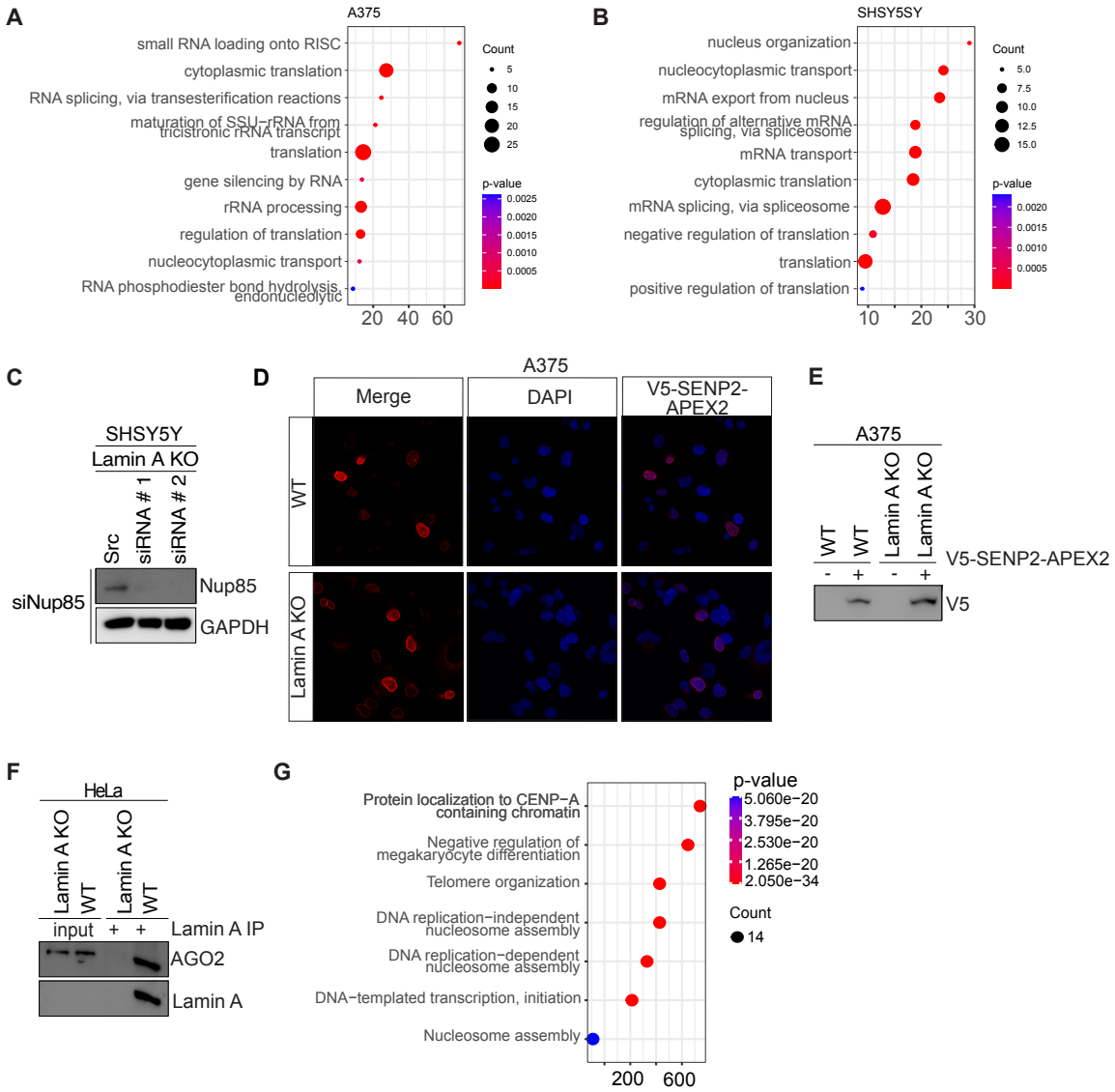

Supplemental Figure 5 related to main Figure 5. Biological process annotations provided by GO for significantly upregulated processes in the Lamin A KO vs WT nuclear AGO IP mass spectrometry hits from **(A)** A375 and **(B)** SHSY5Y cells. **(C)** Representative images of Nup85 immunoblots SHSY5Y Lamin A KO cells transfected with siRNAs against Nup85. GAPDH was used as a loading control. **(D)** Immunofluorescence staining of V5-SENP2-APEX2 in A375 WT APEX-SENP2 and A375 Lamin A KO APEX2-SENP2 cells. **(E)** Representative image of V5 immunoblot of A375 WT APEX-SENP2 and A375 Lamin A KO APEX2-SENP2 cells as compared to parental cell lines. **(F)** Representative images of AGO2 and Lamin A immunoblots of co-immunoprecipitation assay in HeLa WT and Lamin A KO cells. **(G)** Biological process annotations by GO for the significantly upregulated processes in Lamin A IP from WT vs Lamin A KO A375 cells. WT, wild-type cells; Lamin A KO, Lamin A knock out cells; siRNA #1/2, cells transfected with siRNAs against Nup85; V5-SENP2-APEX2, cells expressing V5-SENP2-APEX2 protein; GO, Gene Ontology.

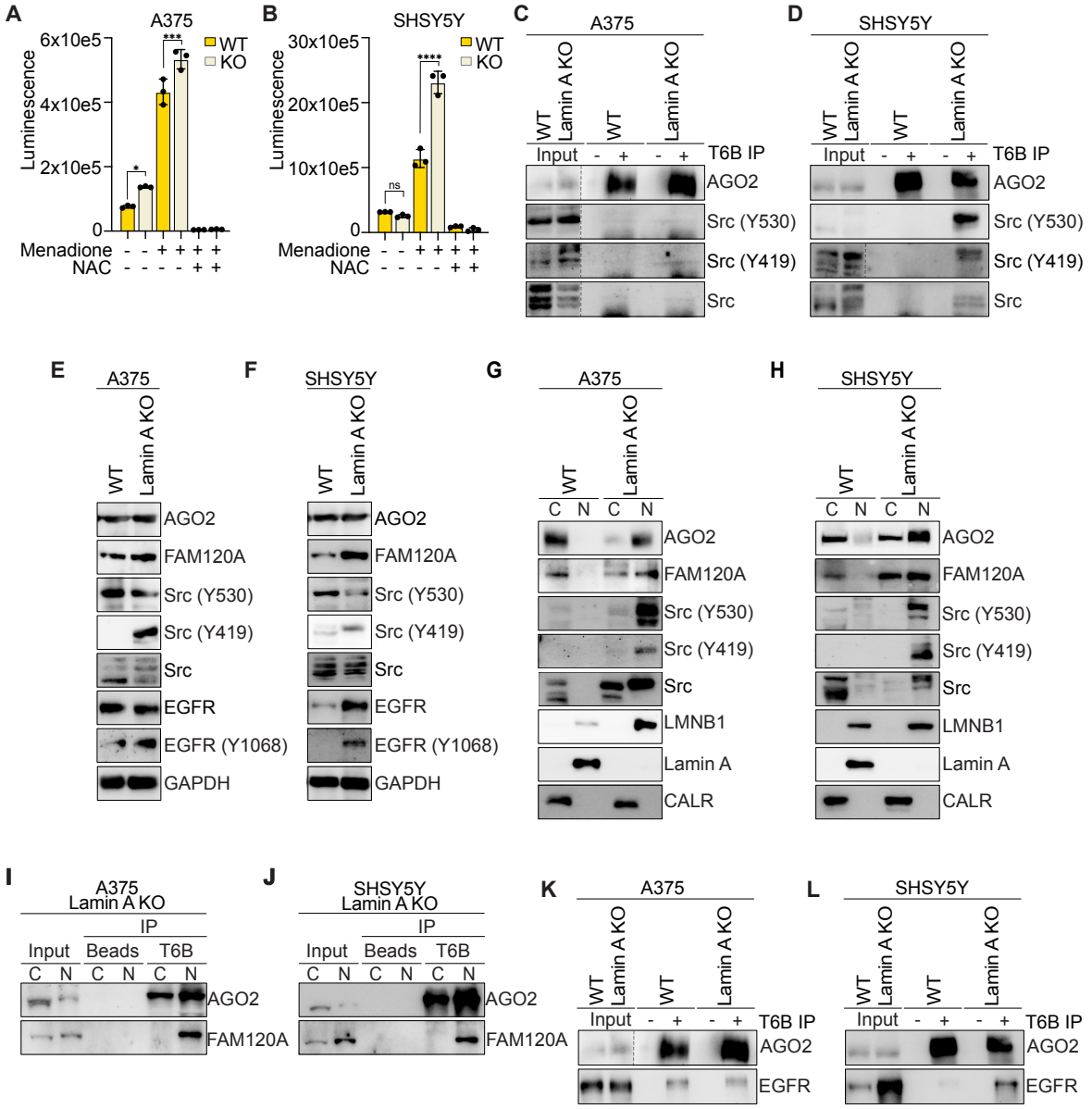

Figure 6. Lamin A KO results in upregulation of oxidative stress and interaction between AGO2 and FAM120A protein. Assessment of H_2O_2 species in the media of Lamin A KO and WT **(A)** A375 and **(B)** SHSY5Y cells after treatment with ROS-inducer (Menadione) or ROS quencher (NAC). Graph present average of three independent experiments, performed in technical triplicates, mean ± standard deviation. Representative images of AGO2, FAM120A, Src, Y1419 Src, Y530 Src immunoblots of AGO2 immunoprecipitation assay in total lysates from **(C)** A375 and **(D)** SHSY5Y WT and Lamin A KO cells. Representative images of AGO2, FAM120A, Y419 Src, Y530 Src, Src, EGFR and Y1068 EGFR immunoblots from total lysates of **(E)** A375 and **(F)** SHSY5Y Lamin A KO and WT cells. GAPDH was used as a loading control. Representative images of AGO2, FAM120A, Y419 Src, Y530 Src, Src, and Lamin A immunoblots from cytoplasmic and nuclear lysates in **(G)** A375 and **(H)** SHSY5Y Lamin A KO and WT cells. CALR served as cytoplasmic marker while LMNB1 served as nuclear marker. Representative images of AGO2 and FAM120A immunoblots from AGO2 immunoprecipitation assay in

cytoplasmic and nuclear lysates from **(I)** A375 and **(J)** SHSY5Y WT and Lamin A KO cells. Representative images of AGO2 and EGFR immunoblots of AGO2 immunoprecipitation assay in total lysates from **(K)** A375 and **(L)** SHSY5Y WT and Lamin A KO cells. WT, wild-type cells; Lamin A KO/KO, Lamin A knock out cells; C, cytoplasmic fraction; N, nuclear fraction; CALR, calreticulin; LMNB1, Lamin B1.

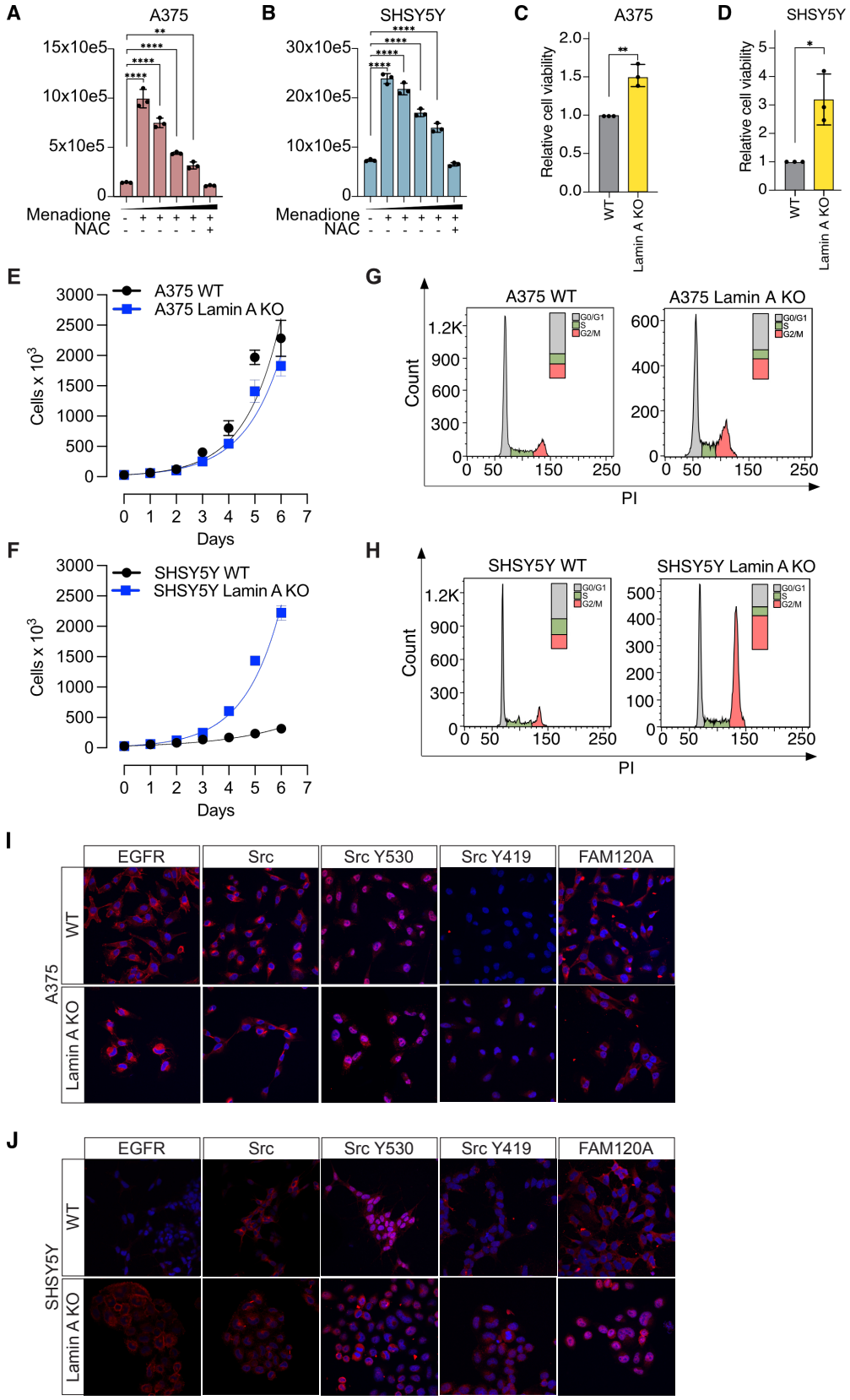

Supplemental Figure 6 related to main Figure 6. Optimization of Menadione concentration in **(A)** A375 and **(B)** SHSY5Y WT cells. Relative viability of Lamin A KO vs WT in **(C)** A375

and **(D)** SHSY5Y cells assessed by MTT assay. Graph present average of three independent experiments, performed in technical triplicates, mean ± standard deviation. Cell proliferation assay for growing Lamin A KO and WT **(E)** A375 and **(F)** SHSY5Y cells. Exponential (Malthusian) growth line for proliferation assays was fitted for the data sets. Results were calculated from four independent experiments performed in technical duplicates and presented as the mean ± standard deviation. Representative histograms of cell cycle analysis by flow cytometry in WT and Lamin A KO growing **(G)** A375 and **(H)** SHSY5Y cells. Immunofluorescence staining of EGFR, Src, Y419 Src, Y530 Src and FAM120A in **(I)** A375 and **(J)** SHSY5Y cells. WT, wild-type cells; Lamin A KO, Lamin A knock out cells. *$P<0.05$, **$P<0.01$,****$P<0,0001$.

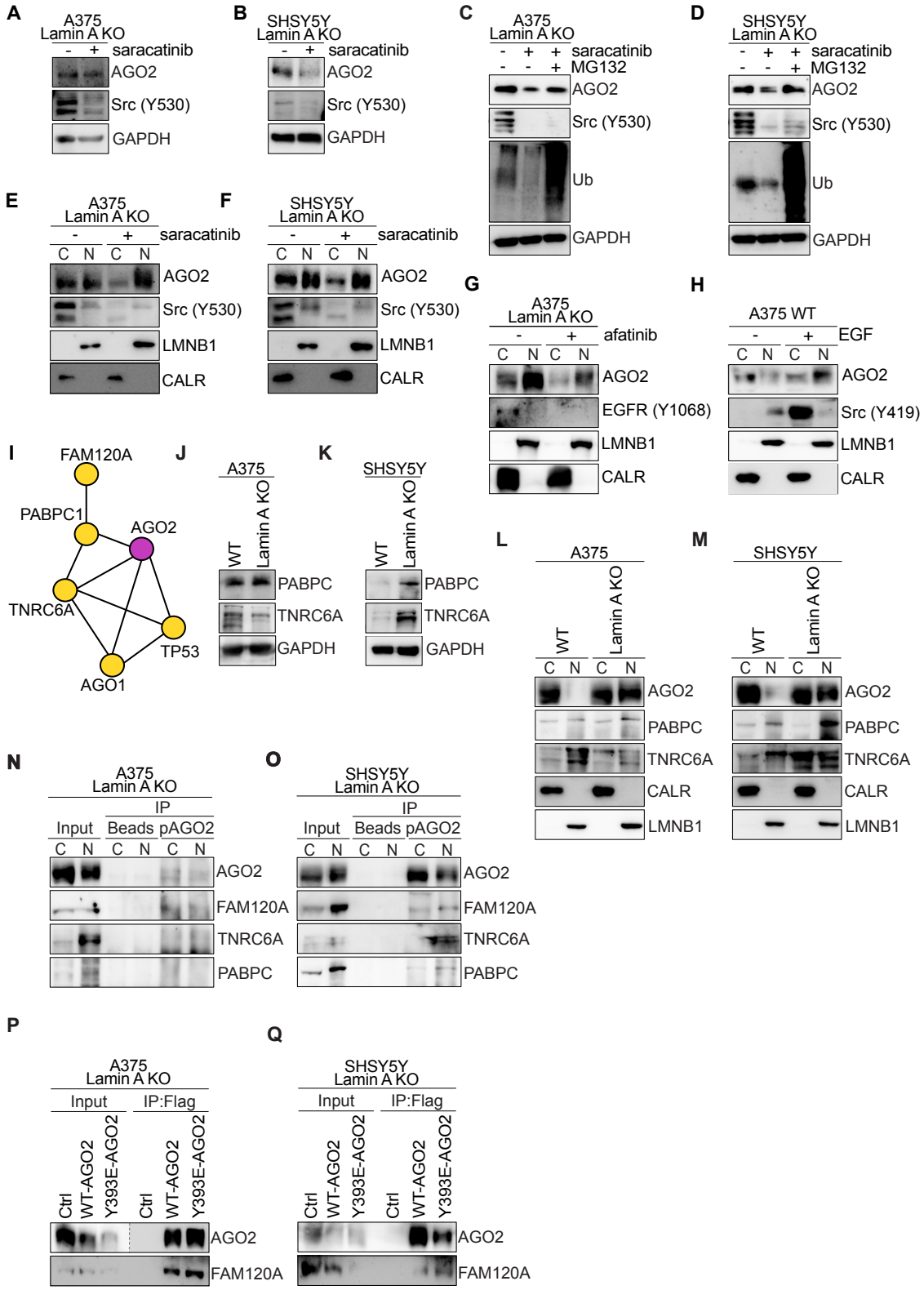

Figure 7. AGO2 levels and subcellular localization are regulated by the EGFR/Src pathway. Representative immunoblots of AGO2 and p530 Src in total lysates of **(A)** A375 and **(B)** SHSY5Y Lamin A KO cells treated with saracatinib. Representative immunoblots of AGO2, Y530 Src and ubiquitinated proteins in total lysates of **(C)** A375 and **(D)** SHSY5Y Lamin A KO cells

treated with saracatinib and/or MG132. GAPDH protein was used as a loading control. Representative images of AGO2 and Y530 Src immunoblots from cytoplasmic and nuclear lysates of **(E)** A375 and **(F)** SHSY5Y Lamin A KO cells treated with saracatinib. **(G)** Representative images of AGO2 and Y1068 EGFR immunoblots from cytoplasmic and nuclear lysates of A375 Lamin A KO cells treated with afatinib. **(H)** Representative images of AGO2 and 419 Src immunoblots from cytoplasmic and nuclear lysates of A375 WT cells treated with EGF. **(I)** String analysis of AGO2 interactome. Representative images of Y393 AGO2, PABPC and TNRC6A immunoblots from total lysates in **(J)** A375 and **(K)** SHSY5Y Lamin A KO and WT cells. CALR served loading control. Representative images of Y393 AGO2, PABPC and TNRC6A immunoblots from cytoplasmic and nuclear lysates in **(L)** A375 and **(M)** SHSY5Y Lamin A KO and WT cells. Calreticulin served as cytoplasmic marker while Lamin B1 served as nuclear marker. Representative images of AGO2, FAM120A, TNRC6A and PABPC immunoblots from pY393 AGO2 immunoprecipitation assay from cytoplasmic and nuclear lysates in **(N)** A375 and **(O)** SHSY5Y WT and Lamin A KO cells. Representative images of AGO2 and FAM120A immunoblots from anti-Flag immunoprecipitation assay in total lysates of Lamin A KO **(P)** A375 and **(Q)** SHSY5Y cells transfected with plasmids containing expression cassettes for either WT-AGO2 or Y393A-AGO2. For biochemical fractionation experiments CALR served as cytoplasmic marker while LMNB1 served as nuclear marker. WT, wild-type cells; Lamin A KO/KO, Lamin A knock out cells; C, cytoplasmic fraction; N, nuclear fraction; CALR, calreticulin; LMNB1, Lamin B1.

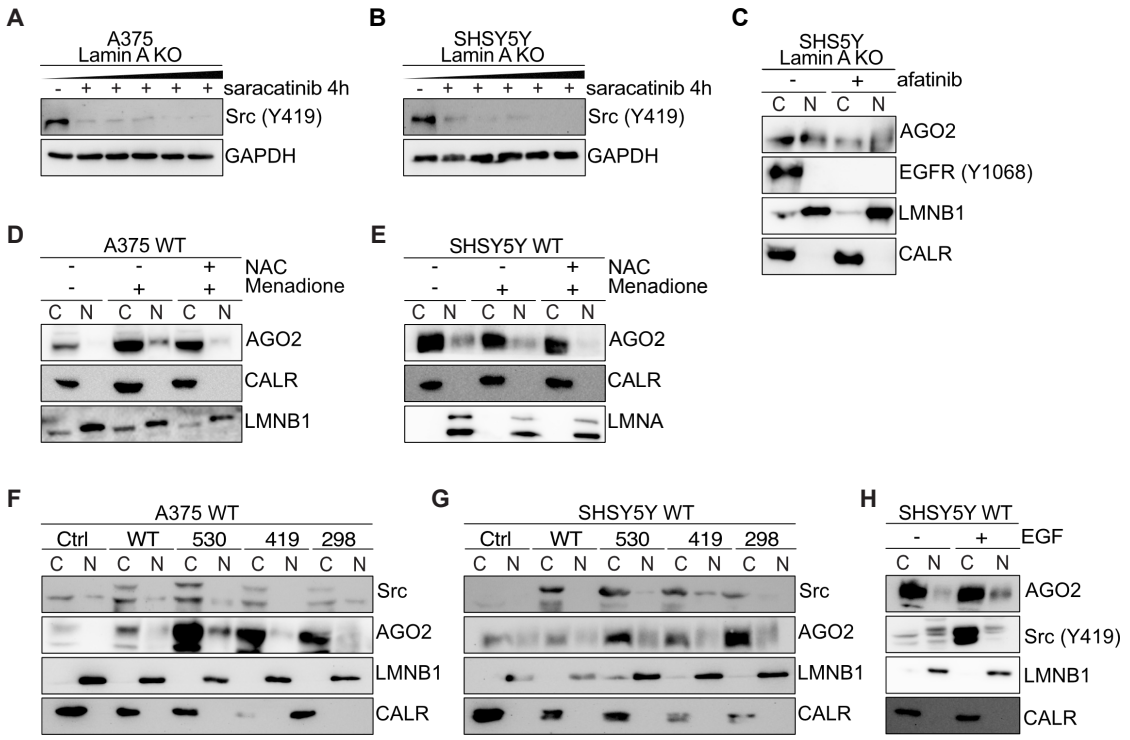

Supplemental Figure 7 related to main Figure 7. Representative immunoblots of AGO2 and p419 Src in total lysates of **(A)** A375 and **(B)** SHSY5Y Lamin A KO cells treated with increasing concentrations of saracatinib. **(C)** Representative images of AGO2 and Y1068 EGFR immunoblots from cytoplasmic and nuclear lysates of SHSY5Y Lamin A KO cells treated with afatinib. Representative images of AGO2 immunoblots from cytoplasmic and nuclear lysates of **(D)** A375 and **(E)** SHSY5Y WT cells treated with Menadione and/or NAC. Representative images of AGO2 and Src immunoblots from cytoplasmic and nuclear lysates of **(F)** A375 and **(G)** SHSY5Y WT cells transfected with WT and mutated Src expression plasmids (constitutively active (Y530F), kinase dead (K298M) and no-dimerization (Y419) mutants). **(H)** Representative images of AGO2 and p419 Src immunoblots from cytoplasmic and nuclear lysates of A375 WT cells treated with EGF. For biochemical fractionation experiments CALR served as cytoplasmic marker while LMNB1 served as nuclear marker. WT, wild-type cells; Lamin A KO/KO, Lamin A knock out cells; C, cytoplasmic fraction; N, nuclear fraction; CALR, calreticulin; LMNB1, Lamin B1.